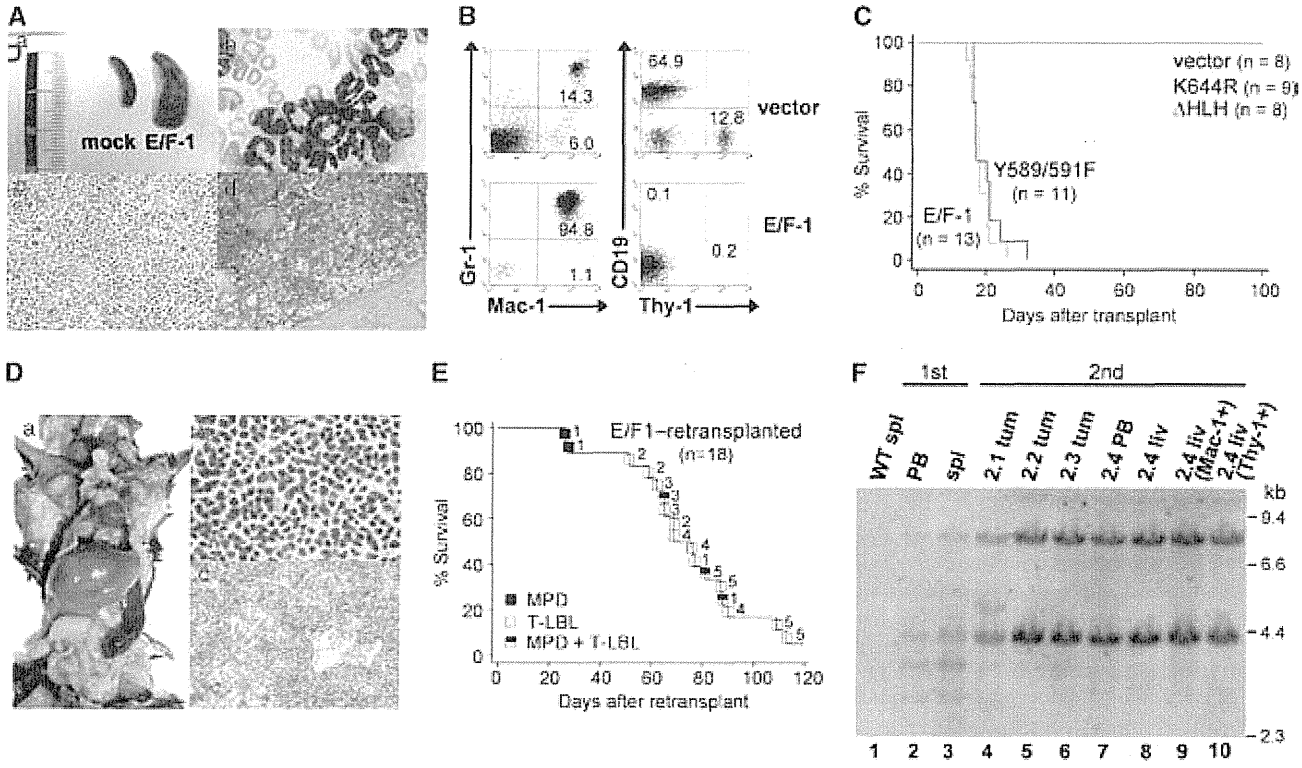

Figure 1. ETV6/FLT3 induces a rapidly fatal MPD in primary recipient mice, which transformed into T-LBL and MPD during serial passage. (**A**) (a) Splenomegaly associated with MPD. (b) Representative May–Giemsa-stained peripheral blood smear of the diseased mouse (× 100). (c, d) Representative hematoxylin and eosin-stained bone marrow (c) and spleen (d) of the diseased mouse (× 20). (**B**) Flow cytometric analysis of cells from the peripheral blood of vector control and E/F-1 mice. The percentages of cells in quadrants of interest are shown. (**C**) Survival curve for recipients of bone marrow transduced with a vector control ($n=8$), E/F-1 ($n=13$), Y589/591F mutant ($n=11$), kinase-inactive K644R mutant ($n=9$) or deletion mutant of the HLH oligomerization domain of ETV6 (ΔHLH) ($n=8$). Mice transplanted with a vector control, K644R, or ΔHLH remain free of disease 180 days after transplant. Survival data are cumulative from two or three separate experiments for all retroviral constructs. (**D**) (a) Macroscopic examination of a secondary recipient with T-LBL (b and c) Hematoxylin and eosin-stained lymph node (b) and liver (c) of the diseased mouse (× 100 and × 20, respectively). (**E**) Kaplan–Meier survival analysis of the secondary recipients. Most secondary recipients succumbed to T-LBL or/and MPD. Pairs of recipients transplanted with cells from the same primary donor are indicated by numbers. (**F**) Proviral integrations in cells isolated from primary and secondary recipients. Genomic DNA isolated from the indicated tissues of a wild-type (WT) mouse (lane 1), a primary MPD mouse (lanes 2 and 3) and four secondary T-LBL mice receiving bone marrow and spleen from the same primary MPD mouse (lanes 4–10) was digested with *Eco*RI and analyzed for proviral integrations by hybridization with a DIG-labeled EGFP probe. Lanes 4–6 are DNAs from the tumors of mice with T-LBL. Lanes 7–10 represent lineage analysis from a single secondary mouse, which developed both MPD and T-LBL (2.4). The peripheral blood of the 2.4 mouse contained 83.5% EGFP$^+$Mac-1$^+$ and 10.6% EGFP$^+$Thy-1$^+$ cells, and the liver of the 2.4 mouse contained 27.2% EGFP$^+$Mac-1$^+$ and 58.8% EGFP$^+$Thy-1$^+$ cells at the time of euthanization. The MACS-sorted liver myeloid (Mac-1$^+$) and T cells (Thy-1$^+$) from this mouse were 98.1% and 98.4% pure, respectively. DNA size markers (in kb) are shown on the right. liv, liver; PB, peripheral blood; spl, spleen; tum, tumor.

were unable to bind Grb2, but not in 2F and 3F-1 mutants (Figure 2d). To examine the contribution of Grb2 binding to ETV6/FLT3-induced MPD *in vivo*, we performed BMT experiments. White blood cell (WBC) counts and spleen weights of the mice receiving 5F-transduced bone marrow were significantly lower than those receiving E/F-1-transduced bone marrow (Supplementary Table S1). Flow cytometric analyses of spleen cells showed that 5F mice had a reduced fraction of Mac-1$^+$/Gr-1$^+$ cells compared with E/F-1 mice (Supplementary Figure S5A). 5F mice showed significantly less infiltrate in the hepatic lobules or periportal areas than the E/F-1 mice (Supplementary Figure S5B). Recipients of both 2F and 3F-1 developed rapidly fatal MPD with a comparable latency to those of E/F-1. Survival of 5F and 3F-2 mice was significantly prolonged compared with that of E/F-1 and E/F-2 mice, respectively (55 days vs 18 days, 73 days vs 13 days, respectively; $P<0.001$; Figure 2e), although most 5F and 3F-2 recipient mice eventually succumbed to MPD.

Finally, we compared the ability of ETV6/FLT3 to transform primary myeloid cells from the bone marrow of Gab2$^{-/-}$ and Gab2$^{+/+}$ mice. Expression of E/F-1 in Gab2$^{-/-}$ cells resulted in an approximately threefold lower number of cytokine-independent CFU-C (Supplementary Figure S6A). We assessed the relative contribution of the *Gab2* gene to ETV6/FLT3-mediated leukemogenesis in BMT experiments using Gab2$^{-/-}$ and Gab2$^{+/+}$ donor mice. All mice transplanted with Gab2$^{+/+}$ bone marrow cells expressing ETV6/FLT3 developed severe MPD (median WBC, $236\times10^3/\mu l$; spleen weight, 561 mg), as expected (Supplementary Figure S6B). ETV6/FLT3-induced myeloproliferation was attenuated in mice transplanted with Gab2$^{-/-}$ bone marrow cells expressing ETV6/FLT3 (median WBC, $31\times10^3/\mu l$; spleen weight, 350 mg). Survival of mice injected with Gab2$^{-/-}$ bone marrow cells expressing E/F-1 was significantly prolonged in comparison with those injected with Gab2$^{+/+}$ cells (56 days vs 21 days, $P<0.001$; Figure 2f), although all recipients of Gab2$^{-/-}$ background bone marrow cells eventually succumbed to MPD.

Our results suggest that ETV6/FLT3 has more potent oncogenic activity than FLT3-ITDs and can transform progenitor cells with the capacity to differentiate into myeloid and lymphoid progeny, supporting the contention that human *ETV6/FLT3*-positive MLN-eo is a stem cell disorder. Unlike FLT3-ITDs, mice that received the

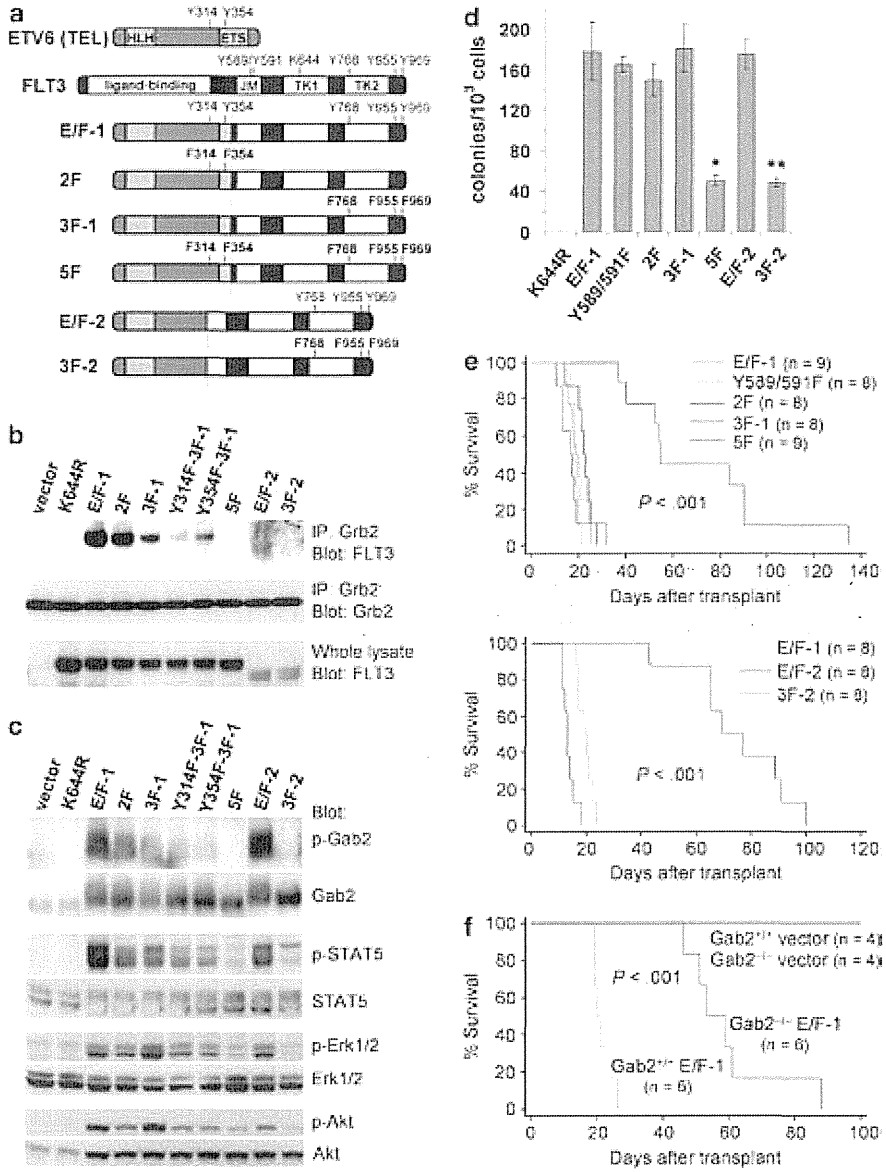

Figure 2. Both ETV6 and FLT3 portions contribute to ETV6/FLT3-mediated leukemogenesis via Grb2-Gab2 pathway. (**a**) Schematic representation of ETV6/FLT3 fusion proteins including the series of Grb2-binding site mutants. The point of fusion is indicated by a vertical dotted line. E/F-1 was cloned by us. E/F-2 was cloned previously (Vu *et al.*[5]). (**b**) Coimmunoprecipitation: lysates from Ba/F3 cells expressing the indicated ETV6/FLT3 proteins were immunoprecipitated using an anti-Grb2 antibody and blotted with anti-FLT3 (top) and anti-Grb2 (middle) antibodies. Whole-cell lysates were also blotted with the anti-FLT3 antibody (bottom). As a control, lysates from vector-transduced cells were included. Three independent experiments were performed and representative data are shown. (**c**) Activation of downstream targets was demonstrated by blotting the whole-cell lysates of Ba/F3 cells with the indicated phosphospecific antibodies. After stripping, the membranes were reprobed with the indicated total antibodies. Three independent experiments were performed and representative data are shown. (**d**) Cytokine-independent colony formation of whole bone marrow cells expressing ETV6/FLT3 wild-type or Grb2-binding mutants. The difference between E/F-1 and 5F (*) and between E/F-2 and 3F-2 (**) is statistically significant ($P<0.001$, unpaired *t*-test). Data are the mean ± s.d. of three independent experiments. (**e**) Survival curve for recipients of bone marrow transduced with ETV6/FLT3 and Grb2-binding mutants. Both E/F-1 and E/F-2 mice caused rapidly fatal MPD. 5F mutant mice and 3F-2 mutant mice developed MPD with a longer median survival of 55 and 73 days, respectively ($P<0.001$ vs E/F-1 and E/F-2, respectively). One of the 5F mutant mice died of severe anemia without showing any signs of MPD. Survival data are cumulative from two or three separate experiments for all retroviral constructs. (**f**) Survival curve for recipients of Gab2$^{-/-}$ and Gab2$^{+/+}$ bone marrow transduced with a vector control or E/F-1. The *P*-value represents a comparison of survival by E/F-1 on Gab2$^{-/-}$ vs Gab2$^{+/+}$ background.

Y589/591F mutant of ETV6/FLT3 also developed a lethal MPD with a short latency. The reason for the discrepancy between ETV6/FLT3 and FLT3-ITDs is not clear. This may be due to altered structural conformation of ETV6/FLT3 relative to wild-type FLT3 or alternatively, it may be due to different subcellular localization of the fusion protein and FLT3-ITDs.[14,15] Recently it was reported that sunitinib and sorafenib, tyrosine kinase inhibitors with multiple targets including FLT3, had therapeutic efficacy in two patients with *ETV6/FLT3*-positive MLN-eo.[6] Unfortunately, similar to most of the patients with *FLT3-ITD*-positive AML, relapse and resistance occurred in both patients. Although clinical application of Grb2 inhibitors remains limited to just a phase I trial of a liposomal antisense for hematological malignancies, the results of the current study indicate therapeutic potential against Grb2 in

patients with *ETV6/FLT3*-positive MLN-eo. In addition, previous studies have shown that the Grb2-Gab2 pathway also has an important role in FLT3-ITD-mediated cell proliferation and survival.[13,15] These findings suggest that inhibition of this pathway may be useful in the treatment of FLT3-associated leukemia.

CONFLICT OF INTEREST

The authors declare no conflict of interest.

ACKNOWLEDGEMENTS

This work was supported in part by grants from the Ministry of Education, Culture, Sports, Science and Technology of Japan (MH).

K Chonabayashi[1], M Hishizawa[1], S Kawamata[2], Y Nagai[1], T Ohno[3], T Ishikawa[1], T Uchiyama[1] and A Takaori-Kondo[1]
[1]Department of Hematology and Oncology, Graduate School of Medicine, Kyoto University, Kyoto, Japan;
[2]Foundation for Biomedical Research and Innovation, Kobe, Japan and
[3]Division of Hematology and Immunology, Department of Internal Medicine, Ohtsu Red Cross Hospital, Ohtsu, Japan
E-mail: hishiza@kuhp.kyoto-u.ac.jp

REFERENCES

1 Stirewalt DL, Radich JP. The role of FLT3 in haematopoietic malignancies. *Nat Rev Cancer* 2003; **3**: 650–665.
2 Kiyoi H, Naoe T, Nakano Y, Yokota S, Minami S, Miyawaki S *et al.* Prognostic implication of FLT3 and N-RAS gene mutations in acute myeloid leukemia. *Blood* 1999; **93**: 3074–3080.
3 Thiede C, Steudel C, Mohr B, Schaich M, Schakel U, Platzbecker U *et al.* Analysis of FLT3-activating mutations in 979 patients with acute myelogenous leukemia: association with FAB subtypes and identification of subgroups with poor prognosis. *Blood* 2002; **99**: 4326–4335.
4 Kindler T, Lipka DB, Fischer T. FLT3 as a therapeutic target in AML: still challenging after all these years. *Blood* 2010; **116**: 5089–5102.
5 Vu HA, Xinh PT, Masuda M, Motoji T, Toyoda A, Sakaki Y *et al.* FLT3 is fused to ETV6 in a myeloproliferative disorder with hypereosinophilia and a t(12;13)(p13;q12) translocation. *Leukemia* 2006; **20**: 1414–1421.
6 Walz C, Erben P, Ritter M, Bloor A, Metzgeroth G, Telford N *et al.* Response of ETV6-FLT3-positive myeloid/lymphoid neoplasm with eosinophilia to inhibitors of FMS-like tyrosine kinase 3. *Blood* 2011; **118**: 2239–2242.
7 Tse KF, Mukherjee G, Small D. Constitutive activation of FLT3 stimulates multiple intracellular signal transducers and results in transformation. *Leukemia* 2000; **14**: 1766–1776.
8 Baldwin BR, Li L, Tse KF, Small S, Collector M, Whartenby KA *et al.* Transgenic mice expressing Tel-FLT3, a constitutively activated form of FLT3, develop myeloproliferative disease. *Leukemia* 2007; **21**: 764–771.
9 Vu HA, Xinh PT, Kano Y, Tokunaga K, Sato Y. The juxtamembrane domain in ETV6/FLT3 is critical for PIM-1 up-regulation and cell proliferation. *Biochem Biophys Res Commun* 2009; **383**: 308–313.
10 Rocnik JL, Okabe R, Yu JC, Lee BH, Giese N, Schenkein DP *et al.* Roles of tyrosine 589 and 591 in STAT5 activation and transformation mediated by FLT3-ITD. *Blood* 2006; **108**: 1339–1345.
11 Tanaka Y, Era T, Nishikawa S, Kawamata S. Forced expression of Nanog in hematopoietic stem cells results in a gammadeltaT-cell disorder. *Blood* 2007; **110**: 107–115.
12 Zhang S, Broxmeyer HE. Flt3 ligand induces tyrosine phosphorylation of gab1 and gab2 and their association with shp-2, grb2, and PI3 kinase. *Biochem Biophys Res Commun* 2000; **277**: 195–199.
13 Masson K, Liu T, Khan R, Sun J, Ronnstrand L. A role of Gab2 association in Flt3 ITD mediated Stat5 phosphorylation and cell survival. *Br J Haematol* 2009; **146**: 193–202.
14 Schmidt-Arras DE, Bohmer A, Markova B, Choudhary C, Serve H, Bohmer FD. Tyrosine phosphorylation regulates maturation of receptor tyrosine kinases. *Mol Cell Biol* 2005; **25**: 3690–3703.
15 Choudhary C, Olsen JV, Brandts C, Cox J, Reddy PN, Bohmer FD *et al.* Mislocalized activation of oncogenic RTKs switches downstream signaling outcomes. *Mol Cell* 2009; **36**: 326–339.

Supplementary Information accompanies this paper on the Leukemia website (http://www.nature.com/leu)

Biochemical and Biophysical Research Communications 425 (2012) 284–289

Contents lists available at SciVerse ScienceDirect

Biochemical and Biophysical Research Communications

journal homepage: www.elsevier.com/locate/ybbrc

NMR study of xenotropic murine leukemia virus-related virus protease in a complex with amprenavir

Ayako Furukawa [a], Hideyasu Okamura [a], Ryo Morishita [b,c], Satoko Matsunaga [c], Naohiro Kobayashi [d], Takahisa Ikegami [d], Tsutomu Kodaki [a,e], Akifumi Takaori-Kondo [f], Akihide Ryo [c], Takashi Nagata [a,e,*], Masato Katahira [a,e,g,*]

[a] Institute of Advanced Energy, Kyoto University, Gokasho, Uji, Kyoto 611-0011, Japan
[b] CellFree Sciences Co. Ltd., Ehime University, Venture Business Laboratory, Matsuyama 790-8577, Japan
[c] Department of Microbiology, Yokohama City University School of Medicine, 3-9 Fukuura, Kanazawa-ku, Yokohama 236-0004, Japan
[d] Institute for Protein Research, Osaka University, 3-2 Yamadaoka, Suita, Osaka 565-0871, Japan
[e] Graduate School of Energy Science, Kyoto University, Gokasho, Uji, Kyoto 611-0011, Japan
[f] Department of Hematology and Oncology, Graduate School of Medicine, Kyoto University, Sakyo-ku, Kyoto 606-8507, Japan
[g] CREST, JST, 5-3 Yonban-cho, Chiyoda-ku, Tokyo 102-8666, Japan

ARTICLE INFO

Article history:
Received 14 July 2012
Available online 25 July 2012

Keywords:
XMRV
Protease
Cell-free protein synthesis
NMR

ABSTRACT

Xenotropic murine leukemia virus-related virus (XMRV) is a virus created through recombination of two murine leukemia proviruses under artificial conditions during the passage of human prostate cancer cells in athymic nude mice. The homodimeric protease (PR) of XMRV plays a critical role in the production of functional viral proteins and is a prerequisite for viral replication. We synthesized XMRV PR using the wheat germ cell-free expression system and carried out structural analysis of XMRV PR in a complex with an inhibitor, amprenavir (APV), by means of NMR. Five different combinatorially ^{15}N-labeled samples were prepared and backbone resonance assignments were made by applying Otting's method, with which the amino acid types of the [^{1}H, ^{15}N] HSQC resonances were automatically identified using the five samples (Wu et al., 2006) [14]. A titration experiment involving APV revealed that one APV molecule binds to one XMRV PR dimer. For many residues, two distinct resonances were observed, which is thought to be due to the structural heterogeneity between the two protomers in the APV:XMRV PR = 1:2 complex. PR residues at the interface with APV have been identified on the basis of chemical shift perturbation and identification of the intermolecular NOEs by means of filtered NOE experiments. Interestingly, chemical shift heterogeneity between the two protomers of XMRV PR has been observed not only at the interface with APV but also in regions apart from the interface. This indicates that the structural heterogeneity induced by the asymmetry of the binding of APV to the XMRV PR dimer is transmitted to distant regions. This is in contrast to the case of the APV:HIV-1 PR complex, in which the structural heterogeneity is only localized at the interface. Long-range transmission of the structural change identified for the XMRV PR complex might be utilized for the discovery of a new type of drug.

1. Introduction

Xenotropic murine leukemia virus-related virus (XMRV) has been implicated in prostate cancer [1] and chronic fatigue syndrome [2]. These reports have attracted much attention since a causal relationship between a retrovirus and a human disease had only been known for HIV and AIDS [3]. After several years of controversial research, a recent study has indicated that XMRV was generated through the recombination of two proviruses during the passaging of human tumors in mice [4]. Thus, XMRV is as not yet regarded as an etiological agent for human diseases, however, it can be considered as a rational example of a gammaretrovirus that can infect human cells and replicate within them.

Proteases (PRs) of viruses such as those of the HIV-1 and hepatitis C ones have been prime targets for antiviral drug development. Although hundreds of inhibitors have been discovered for HIV-1 PR for example, only a few of them are potent antiprotease drugs that are in clinical use [5]. Additionally, long-term administration of these drugs causes the emergence of drug-resistant mutants [6]. It is expected that a detailed description of the interaction between a newly found protease of the retrovirus

* Corresponding authors. Address: Institute of Advanced Energy, Kyoto University, Gokasho, Uji, Kyoto 611-0011, Japan (M. Katahira).
E-mail addresses: nagatat@iae.kyoto-u.ac.jp (T. Nagata), katahira@iae.kyoto-u.ac.jp (M. Katahira).

0006-291X/$ - see front matter © 2012 Elsevier Inc. All rights reserved.
http://dx.doi.org/10.1016/j.bbrc.2012.07.083

family and its cognate substrate or inhibitor may provide valuable information.

XMRV PR is a homodimer, each subunit (protomer) comprising 125 amino acids with a single catalytic Asp residue [7,8]. XMRV PR processes viral polyproteins to yield mature proteins required in the viral life cycle, as is the case for HIV-1 PR. The sequence identity between and similarity of these two proteins are 21% and 27%, respectively, over 99 amino acid residues with a single gap (sequences aligned with ClustalW2 [9,10]). The crystal structures of XMRV PR have been solved in both the free form and complex forms with several inhibitors [7,8]. The fold of XMRV PR is similar to that of HIV-1 PR. The overall structural similarity between the protomer of XMRV PR (PDB ID: 3NR6; [7]) and that of HIV-1 PR (99 amino acids; PDB ID: 3HVP; [11]) in the free form was found to be 1.04 Å of RMSD over 53 C^{α} atoms (calculated using CHIMERA [12]).

In the present study, we used our established wheat germ protein production system to obtain otherwise cell-toxic XMRV PR [13]. This system allowed us to obtain not only a large amount of free and amprenavir (APV)-bound XMRV PR, but also uniformly and combinatorially isotope-labeled samples. The latter isotope-labeled samples made it possible to apply Otting's rapid assignment strategy [14] in combination with conventional protocols [15]. It was critical to utilize this strategy for accomplishment of the assignments. We found that the asymmetry of the binding for the APV:XMRV PR = 1:2 complex results in the structural heterogeneity between the two protomers of XMRV PR at the interface, and, but more importantly, in regions distant from the interface. In the case of the binding of APV to HIV-1 PR, in contrast, the asymmetry causes structural heterogeneity only at the interface.

2. Materials and methods

2.1. Sample preparation

XMRV PR comprising 1–125 residues with an additional threonine residue at the C-terminal end, was synthesized by means of our wheat germ cell-free expression system as an N-terminal glutathione-S-transferase (GST) fusion protein. The XMRV PR fragment was cloned by PCR from the XMRV VP62 clone [16,17] (UniProt ID: A1Z651) and subcloned into pEU-E01-GW [18] with the DNA sequences of the GST gene and Tobacco Etch Virus Protease (TEV) cleavage site. This plasmid DNA was subjected to *in vitro* transcription and cell-free protein synthesis with the wheat germ protein production system [13]. Cell-free protein production was carried out using the ENDEXT.AN. Wheat Germ Expression Kit and according to the instructions provided by the supplier (CellFree Sciences Co. Ltd., Matsuyama, Japan). The cell-free protein production and cleavage purification were also carried out using an automatic robot, Protemist DTII (CellFree Sciences Co. Ltd.), basically according to manufacturer's instructions. GST-XMRV PR was synthesized either in the absence or presence of APV. After the synthesis, the protein solution was loaded onto a Glutathione-Sepharose 4B column (GE Healthcare), and the bound GST-XMRV PR was washed thoroughly with PBS buffer. Subsequently, GST-fused TEV protease (Nacalai Tesque) was applied to cleave the XMRV PR off on-column. The XMRV PR was then collected and dialyzed against either 20 mM sodium phosphate (pH 6.5), 50 mM NaCl and 10 μM APV for the APV-bound XMRV PR or 20 mM Tris–HCl (pH 8.0) and 50 mM NaCl for APV-free XMRV PR. As substrates for protein synthesis, isotropically labeled amino acids were used to synthesize uniformly ^{15}N- and ^{15}N, ^{13}C-labeled ([U-^{15}N] and [U-^{13}C, U-^{15}N], respectively) XMRV PRs. Five different combinatorially ^{15}N-labeled samples of XMRV PR were prepared following Otting's labeling scheme, as shown in Fig. 1C [14].

2.2. NMR spectroscopy

For XMRV PR in a complex with APV, NMR spectra were acquired at 22.9 °C using Bruker 600 and 950 MHz spectrometers each equipped with a cryoprobe. Data were processed and analyzed using NMRPipe [19] and Kujira [20]. The sample solutions comprised 0.1–0.3 mM protein in a complex with APV, 20 mM sodium phosphate (pH 6.5), 50 mM NaCl, 10 μM APV, and 5% D_2O. The amino acid in [^{1}H, ^{15}N] HSQC spectra were identified using the five different combinatorially ^{15}N-labeled samples according to Wu et al. [14]. Sequential assignments of the main chain resonances were made by means of conventional triple resonance experiments [15,21,22]. The main chain $^{1}H^{N}$ and ^{15}N chemical shift heterogeneity between the two protomers in the APV:XMRV PR = 1:2 complex was defined as $\{(\Delta\delta^{1}H^{N})^2 + (\Delta\delta^{15}N/5)^2\}^{1/2}$, where $\Delta\delta^{1}H^{N}$ and $\Delta\delta^{15}N$ are the chemical shift differences between the two protomers for $^{1}H^{N}$ and ^{15}N resonances, respectively. The secondary structures of XMRV PR in a complex with APV was identified based on $^{13}C^{\alpha}$, $^{13}C^{\beta}$ and $^{13}C'$ chemical shift values [23]. The intermolecular NOEs between XMRV PR and APV were obtained from 2D [F1, F2] ^{13}C, ^{15}N-filtered NOESY (120 ms mixing time), 2D [F2] ^{13}C, ^{15}N-filtered NOESY (120 ms mixing time), 3D [F1] ^{13}C, ^{15}N-filtered, [F2] ^{13}C-edited NOESY (120 ms mixing time) [24], and 3D ^{13}C-edited NOESY (78 ms mixing time) spectra.

For free XMRV PR, NMR spectra were acquired at 15.0 °C using a Bruker 600 MHz spectrometer equipped with a cryoprobe. The sample solutions comprised ~0.1 mM protein, 20 mM Tris–HCl (pH 8.0), 50 mM NaCl and 5% D_2O. Partial assignments of the main chain $^{1}H^{N}$ and ^{15}N resonances were made using 3D ^{15}N-edited NOESY spectra utilizing on the assignments for the XMRV PR–APV complex as a reference. The main chain $^{1}H^{N}$ and ^{15}N chemical shift perturbations between the free and APV-bound forms of XMRV PR were defined as $\{(\Delta\delta^{1}H^{N})^2 + (\Delta\delta^{15}N/5)^2\}^{1/2}$, where $\Delta\delta^{1}H^{N}$ and $\Delta\delta^{15}N$ are the chemical shift differences between the free and APV-bound forms for $^{1}H^{N}$ and ^{15}N resonances, respectively. For the APV-bound form, the average of the chemical shift values for the two protomers was used to calculate the differences.

3. Results and discussion

3.1. Characteristics of the [^{1}H, ^{15}N] HSQC spectrum of the XMRV PR in complex with APV

We have successfully obtained cell-toxic XMRV PR by using a cell-free protein synthesis system in both the presence and absence of APV. Moreover, we were able to prepare [U-^{15}N] and [U-^{13}C, U-^{15}N] labeled, and five different combinatorially ^{15}N-labeled samples of XMRV PR, all of which critically facilitated our NMR analyses.

First, titration with APV was carried out. Disappearance of the resonances of XMRV PR in the free state and simultaneous appearance of new resonances for the APV-bound form were observed in the [^{1}H, ^{15}N] HSQC spectrum during the titration. This indicates that the free and bound forms of XMRV PR are in a slow exchange regime on an NMR time scale. Such spectral changes for XMRV PR were seen until APV:XMRV PR = 1:2, but no further change was seen on further addition of APV. This indicates that the stoichiometry is one APV molecule per one XMRV PR dimer (two XMRV PR monomers).

Each protomer comprises 126 amino acid residues, including 12 proline ones. If the homodimer exhibits symmetry, maximally 113 backbone resonances are expected to be observed, because those of the N-terminus and proline residues do not appear. However, the [^{1}H, ^{15}N] HSQC spectrum contained more than 1.5-times as many

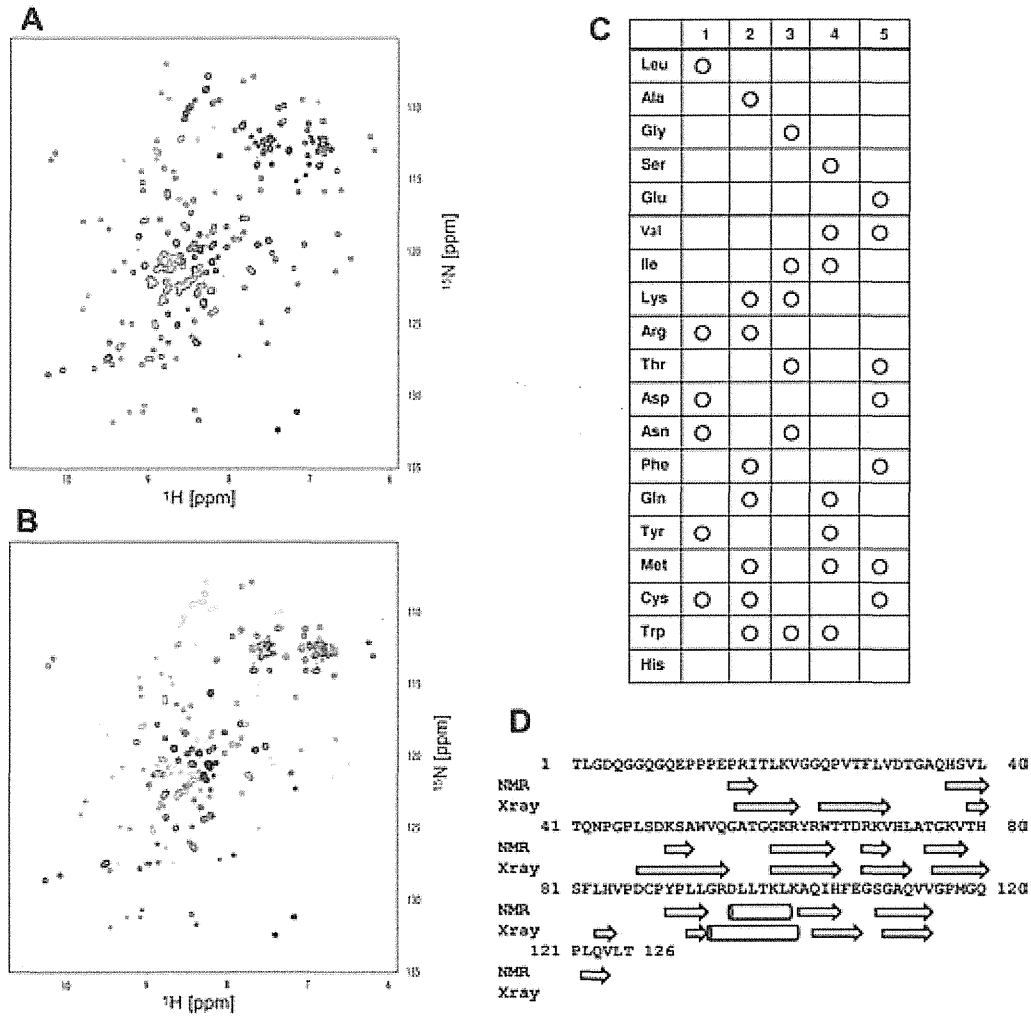

Fig. 1. (A) [^{1}H, ^{15}N] HSQC spectrum of uniformly ^{13}C, ^{15}N-labeld XMRV PR in a complex with APV. (B) Superposition of the [^{1}H, ^{15}N] HSQC spectra of five different combinatorially ^{15}N-labeled XMRV PRs (1–5 of (C)) in a complex with APV, colored red, cyan, green, magenta and blue, respectively. (C) Five different combinatorial labeling schemes [14]. (D) Comparison of the secondary structures of XMRV PR in a complex with APV between the crystal [8] and solution (this work) states. (For interpretation of the references to colour in this figure legend, the reader is referred to the web version of this article.)

backbone resonances as expected (Fig. 1A). This observation reveals that the APV-bound XMRV PR exhibits asymmetry.

3.2. Sequence-specific resonance assignments and identification of the secondary structure of the XMRV PR in a complex with APV

We applied Otting's strategy, with which amino acids could be automatically identified on the basis of the comparison of five spectra [14]. Assignments of the $^{1}H^{N}$, ^{15}N, $^{13}C^{\alpha}$, $^{13}C^{\beta}$, and $^{13}C'$ backbone resonances of XMRV PR in complex with APV were carried out with the knowledge of the amino acid. Almost all of the observed resonances were successfully assigned. It was found that two distinct backbone resonances were observed for many residues of XMRV PR in a complex with APV, which resulted in more than 1.5 times as many backbone resonances as expected. The observation of two distinct peaks for many residues must be due to that the two protomers of the XMRV PR dimer are not identical to each other in the APV:XMRV PR = 1:2 complex.

The secondary structure of the XMRV PR in a complex with APV was identified according to the $^{13}C^{\alpha}$, $^{13}C^{\beta}$ and $^{13}C'$ chemical shift values [23] (Fig. 1D). It was noticed that the two protomers exhibited almost identical secondary structures. The solution structure of XMRV PR in a complex with APV turned out to be basically the same as the crystal structure, which was solved recently [8], as shown in Fig. 1D.

3.3. Binding mode of APV as to XMRM PR in solution

The quality of the [^{1}H, ^{15}N] HSQC spectrum of APV-free XMRV PR appeared to be rather poor due to line broadening of resonances in comparison with in the case of APV-bound XMRV PR. By comparing the spectral patterns of the 3D ^{15}N-edited NOESY spectra between the APV-bound and APV-free forms of XMRV PR, we achieved partial assignment of the main chain $^{1}H^{N}$ and ^{15}N resonances of APV-free XMRV PR. It was found on this analysis that only one set of resonances was observed for APV-free XMRV PR. This indicates that the two protomers are symmetric as to each other in the APV-free form. We then calculated the chemical shift perturbations of the backbone resonances of XMRV PR upon APV binding, and mapped them onto the crystal structure (Fig. 2A). The largest perturbations were observed for the residues located close to APV in the crystal structure (Fig. 2A). This strongly suggests that in solution APV resides at a similar position to as observed in the crystal.

In order to further confirm the interface of XMRV PR with APV, identification of intermolecular NOEs was attempted. First, the $^{1}H^{N}$

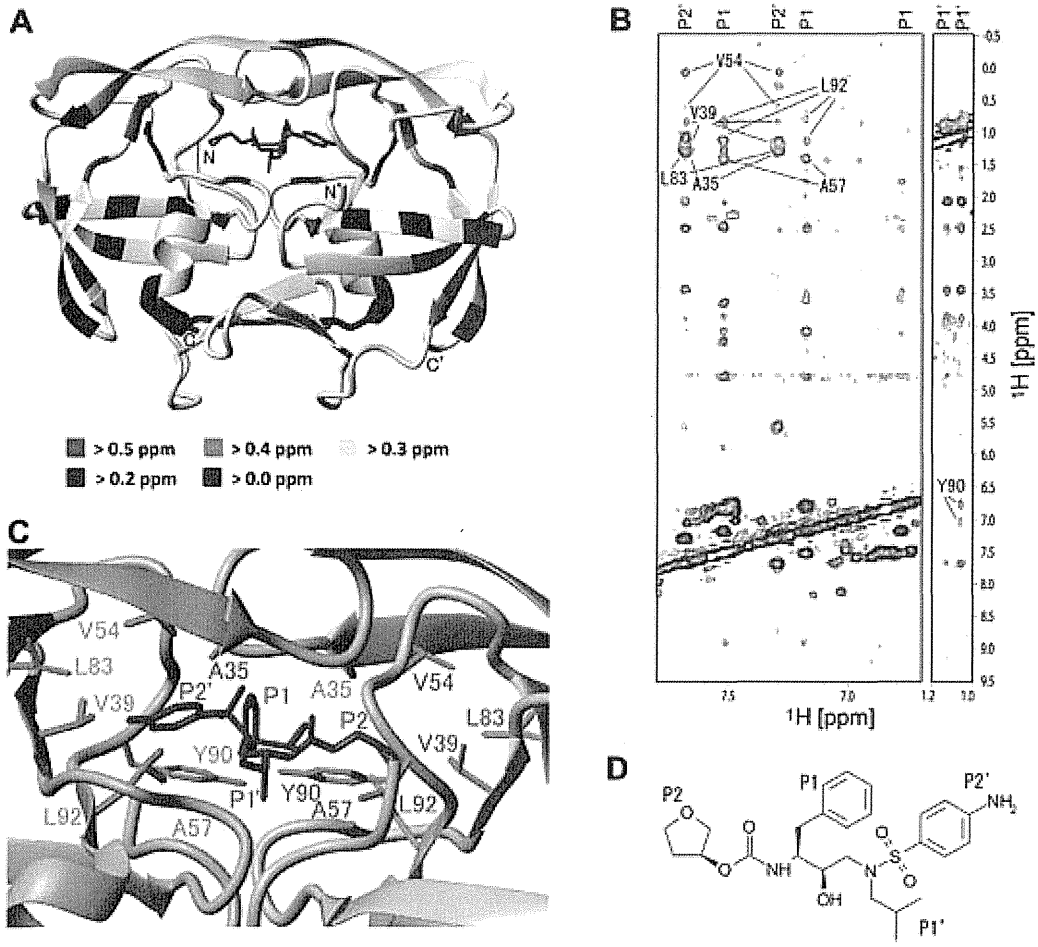

Fig. 2. (A) Mapping of the $^{1}H^{N}$, ^{15}N chemical shift perturbations between the APV-free and APV-bound forms of XMRV PR onto the crystal structure of the APV:XMRV PR complex (PDB accession number 3SM2). The N- and C-termini of the two protomers are denoted by N and C, and N′ and C′, respectively. (B) 2D [F2] ^{13}C, ^{15}N-filtered NOESY (120 ms mixing time) (blue) and 2D [F1, F2] ^{13}C, ^{15}N-filtered NOESY (120 ms mixing time) (red) of XMRV PR in a complex with APV. The assigned intermolecular NOE peaks for XMRV PR and APV are labeled. (C) APV bound to XMRV PR in the crystal (PDB accession number 3SM2). The protomers of XMRV PR are shown in yellow and gray, respectively. APV, is colored magenta. (D) Chemical structure of APV. (For interpretation of the references to colour in this figure legend, the reader is referred to the web version of this article.)

resonances of APV bound to XMRV PR were assigned using the 2D [F1, F2] ^{13}C, ^{15}N-filtered NOESY spectrum (Fig. 2B). Secondly, the intermolecular NOEs between XMRV PR and APV were discriminated by comparing the 2D [F1, F2] ^{13}C, ^{15}N-filtered NOESY and 2D [F2] ^{13}C, ^{15}N-filtered NOESY spectra (Fig. 2B). That is, NOEs observed in the latter spectrum but not in the former one were judged to be intermolecular NOEs. Finally, these intermolecular NOEs were assigned by combinational use of the 3D [F1] ^{13}C, ^{15}N-filtered, [F2] ^{13}C-edited NOESY, 3D ^{13}C-edited NOESY, and 3D ^{15}N-edited NOESY spectra. Consequently, we were able to identify and assign the intermolecular NOEs between APV (P1, P1′, P2 and P2′), and either the methyl groups of A35, V39, V54, A57, L83 and L92 or the aromatic ring of Y90 (Fig. 2B). These intermolecular NOEs turned out to be fully consistent with the crystal structure of the APV:XMRV PR complex. All of the listed amino acid residues are indeed located close to APV in the crystal structure (Fig. 2C). This revealed that in solution APV binds to XMRV in the same manner as observed in the crystal.

3.4. Long-range transmission of the structural heterogeneity between two protomers in the APV:XMRV PR complex

The $^{1}H^{N}$, ^{15}N chemical shift heterogeneity of the backbone resonances between the two protomers of XMRV PR in a complex with APV was calculated and mapped onto the crystal structure of the XMRV PR:APV complex (Fig. 3A). It turned out that chemical shift heterogeneity was observed not only at the APV-binding site (D32, A35, Q36 and L92), but also at positions distant from the APV-binding site (S38, L73, H80, S81, L97 and L122). This suggests that the structural heterogeneity occurs not only at the interface with APV but also in these regions in the APV:XMRV PR = 1:2 complex.

Then, we examined the structural heterogeneity of the crystal structure of the APV:XMRV PR complex. The backbone atoms of the two protomers were superimposed and the differences in position between the C^{α} atoms of the two protomers were calculated to estimate the structural heterogeneity in the crystal. The C^{α}–C^{α} distance was mapped on the crystal structure of the APV:XMRV PR complex (Fig. 3B). It is found that structural heterogeneity is present not only at the interface with APV but also in regions distant in the crystal structure too. Thus, it was found that the structural heterogeneity exhibits long-range transmission in the APV:XMRV PR = 1:2 complex in both solution and crystal states.

3.5. Long-range transmission of the structural heterogeneity is specific to the APV:XMRV PR complex, not being observed in the APV:HIV-1 PR complex

Next, we examined if the long-range transmission of the structural heterogeneity occurs for PR of another virus, HIV-1. The $^{1}H^{N}$, ^{15}N chemical shift heterogeneity between the two protomers of

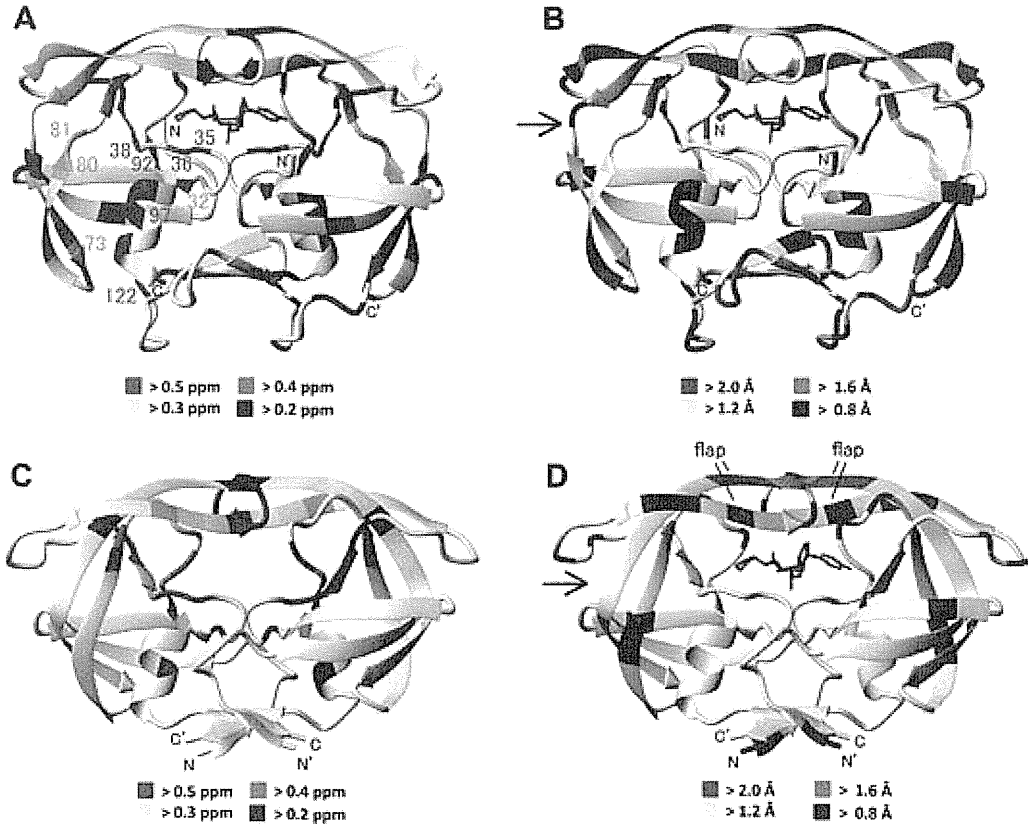

Fig. 3. (A) Mapping of the $^{1}H^{N}$, ^{15}N chemical shift heterogeneity between the two protomers of XMRV PR in a complex with APV onto the crystal structure of the XMRV PR–APV complex (PDB accession number 3SM2). (B) Mapping of the C^{α}–C^{α} distance between the two superimposed protomers of the XMRV PR–APV crystal structure. The shallow groove is indicated by an arrow. (C) Mapping of the $^{1}H^{N}$, ^{15}N chemical shift heterogeneity between the two protomers of the HIV PR (D25N) in a complex with a peptide substrate [25] onto the crystal structure of the HIV PR (D25N)–APV complex. The structure of APV has been deleted. (D) Mapping of the C^{α}–C^{α} distance between the two superimposed protomers in the HIV PR (D25N)–APV crystal structure. The shallow groove is indicated by an arrow. The flap is also indicated.

HIV-1 (D25N) PR in a complex with a peptide substrate was calculated using the previously reported data [25]. Here, heterogeneity in solution was analyzed for the peptide-bound form, because NMR data on HIV-1 in a complex with APV are not available. It has been confirmed that the mutant (D25N) and wild-type HIV-1 PRs exhibited essentially identical backbone chemical shift values, except for those of mutated residue 25 and adjacent residues [25]. Since the peptide substrate is larger than APV in size and has a highly asymmetric structure, this system could be used instead to compare the heterogeneity between the XMRV and HIV-1 PRs. The chemical shift heterogeneity values were mapped onto the crystal structure of the HIV-1 PR (D25N) in a complex with APV (Fig. 3C). The chemical shift heterogeneity was mostly observed for residues located close the substrate/inhibitor-binding site. This indicates that the structural heterogeneity is localized around the substrate binding site and that the structural heterogeneity is not transmitted to distant regions in the HIV-1 PR, which is in contrast to the case of the XMRV PR.

In order to further confirm the localization of the structural heterogeneity for HIV-1 PR, the crystal structure of the APV:HIV-1 PR (D25N) complex was examined. The differences in the positions of the C^{α} atoms of the two protomers were calculated and mapped onto the crystal structure (Fig. 3D). The structural heterogeneity was mostly observed for the residues that are close to the substrate-binding site. This is consistent with the conclusion derived from NMR data in solution for HIV-1 PR. Thus, the long-range transmission of the structural heterogeneity does not occur in HIV-1 PR, but is specific to XMRV-PR.

3.6. Implications for discovery of new types of drug on the basis of the identification of long-range transmission of the structural heterogeneity

It has been pointed out for HIV-1 PR that opening and closing of the flap of the binding site results in compression and expansion of the shallow groove indicated by the arrow in Fig. 3D, respectively [26,27]. Recently, the peripheral surface of HIV-1 PR, which is relatively apart from the binding site, was suggested to be a good target for the discovery of allosteric inhibitors. A fragment-based screen against HIV-1 PR in a complex with TL-3, a universal inhibitor of retroviral PRs, has been employed using the Active Sight fragment library and X-ray crystallography [28]. The authors of that study discovered that 2-methylcyclohexanol binds to the 'exo site' just by the shallow groove [28]. This compound binds to the shallow groove and restricts its compression, and thus prevents the flap from opening. Therefore, it was proposed that the compound can be used as a starting molecule for the development of high-affinity allosteric inhibitors [28]. This example illustrates that a drug that binds to a position distant from the binding site can affect the binding affinity, being a candidate inhibitor. We have shown that the structural heterogeneity is transmitted away in XMRV PR. This means that the heterogeneous structural changes on binding of APV are transmitted to distant regions. This implies conversely that a drug that binds to a distant site may affect the structure of the substrate-binding site and thus inhibit binding of a substrate. This new type of a drug might be discovered more easily for XMRV PR than for HIV-1 PR. Then, in some cases, the discovered drug might

bind to only one protomer of the dimer due to structural heterogeneity, as is the case for 2-methylcyclohexanol [28].

Acknowledgments

This work was supported by Grants from MEXT (23570146, 23657072, 24121714, and 24113710), JST-SENTAN, JST-CREST, the Sumitomo-Denko Foundation and the Iwatani Foundation. This work was performed using the NMR spectrometer with the ultra-high magnetic field under the Cooperative Research Program of Institute for Protein Research, Osaka University.

References

[1] R. Schlaberg, D.J. Choe, K.R. Brown, H.M. Thaker, I.R. Singh, XMRV is present in malignant prostatic epithelium and is associated with prostate cancer, especially high-grade tumors, Proc. Natl. Acad. Sci. USA 106 (2009) 16351–16356.

[2] V.C. Lombardi, F.W. Ruscetti, J. Das Gupta, M.A. Pfost, K.S. Hagen, D.L. Peterson, S.K. Ruscetti, R.K. Bagni, C. Petrow-Sadowski, B. Gold, M. Dean, R.H. Silverman, J.A. Mikovits, Detection of an infectious retrovirus, XMRV, in blood cells of patients with chronic fatigue syndrome, Science 326 (2009) 585–589.

[3] S. Broder, R.C. Gallo, A pathogenic retrovirus (HTLV-III) linked to AIDS, N. Engl. J. Med. 311 (1984) 1292–1297.

[4] T. Paprotka, K.A. Delviks-Frankenberry, O. Cingoz, A. Martinez, H.J. Kung, C.G. Tepper, W.S. Hu, M.J. Fivash Jr., J.M. Coffin, V.K. Pathak, Recombinant origin of the retrovirus XMRV, Science 333 (2011) 97–101.

[5] I.R. Singh, J.E. Gorzynski, D. Drobysheva, L. Bassit, R.F. Schinazi, Raltegravir is a potent inhibitor of XMRV, a virus implicated in prostate cancer and chronic fatigue syndrome, PLoS ONE 5 (2010) e9948.

[6] E.J. Arts, D.J. Hazuda, HIV-1 antiretroviral drug therapy, Cold Spring Harb. Perspect. Med. 2 (2012) a007161.

[7] M. Li, F. Dimaio, D. Zhou, A. Gustchina, J. Lubkowski, Z. Dauter, D. Baker, A. Wlodawer, Crystal structure of XMRV protease differs from the structures of other retropepsins, Nat. Struct. Mol. Biol. 18 (2011) 227–229.

[8] M. Li, A. Gustchina, K. Matuz, J. Tozser, S. Namwong, N.E. Goldfarb, B.M. Dunn, A. Wlodawer, Structural and biochemical characterization of the inhibitor complexes of xenotropic murine leukemia virus-related virus protease, FEBS J. 278 (2011) 4413–4424.

[9] M. Goujon, H. McWilliam, W. Li, F. Valentin, S. Squizzato, J. Paern, R. Lopez, A new bioinformatics analysis tools framework at EMBL-EBI, Nucleic Acids Res. 38 (2010) W695–699.

[10] M.A. Larkin, G. Blackshields, N.P. Brown, R. Chenna, P.A. McGettigan, H. McWilliam, F. Valentin, I.M. Wallace, A. Wilm, R. Lopez, J.D. Thompson, T.J. Gibson, D.G. Higgins, Clustal W and Clustal X version 2.0, Bioinformatics 23 (2007) 2947–2948.

[11] A. Wlodawer, M. Miller, M. Jaskolski, B.K. Sathyanarayana, E. Baldwin, I.T. Weber, L.M. Selk, L. Clawson, J. Schneider, S.B. Kent, Conserved folding in retroviral proteases: crystal structure of a synthetic HIV-1 protease, Science 245 (1989) 616–621.

[12] E.F. Pettersen, T.D. Goddard, C.C. Huang, G.S. Couch, D.M. Greenblatt, E.C. Meng, T.E. Ferrin, UCSF Chimera – a visualization system for exploratory research and analysis, J. Comput. Chem. 25 (2004) 1605–1612.

[13] S. Matsunaga, T. Sawasaki, H. Ode, R. Morishita, A. Furukawa, R. Sakuma, W. Sugiura, H. Sato, M. Katahira, A. Takaori-Kondo, N. Yamamoto, A. Ryo, Molecular and enzymatic characterization of XMRV protease by a cell-free proteolytic analysis, J. Proteomics (2012).

[14] P.S. Wu, K. Ozawa, S. Jergic, X.C. Su, N.E. Dixon, G. Otting, Amino-acid type identification in ^{15}N-HSQC spectra by combinatorial selective ^{15}N-labelling, J. Biomol. NMR 34 (2006) 13–21.

[15] J. Cavanagh, W.J. Fairbrother, A.G. Palmer, N.J. Skelton, M. Rance, Protein NMR Spectroscopy: Principles and Practice, second ed., Academic Press, San Diego, CA, 2007.

[16] R. Sakuma, T. Sakuma, S. Ohmine, R.H. Silverman, Y. Ikeda, Xenotropic murine leukemia virus-related virus is susceptible to AZT, Virology 397 (2010) 1–6.

[17] A. Urisman, R.J. Molinaro, N. Fischer, S.J. Plummer, G. Casey, E.A. Klein, K. Malathi, C. Magi-Galluzzi, R.R. Tubbs, D. Ganem, R.H. Silverman, J.L. DeRisi, Identification of a novel Gammaretrovirus in prostate tumors of patients homozygous for R462Q RNASEL variant, PLoS Pathog. 2 (2006) e25.

[18] H. Takahashi, A. Nozawa, M. Seki, K. Shinozaki, Y. Endo, T. Sawasaki, A simple and high-sensitivity method for analysis of ubiquitination and polyubiquitination based on wheat cell-free protein synthesis, BMC Plant Biol. 9 (2009).

[19] F. Delaglio, S. Grzesiek, G.W. Vuister, G. Zhu, J. Pfeifer, A. Bax, NMRPipe: a multidimensional spectral processing system based on UNIX pipes, J. Biomol. NMR 6 (1995) 277–293.

[20] N. Kobayashi, J. Iwahara, S. Koshiba, T. Tomizawa, N. Tochio, P. Guntert, T. Kigawa, S. Yokoyama, KUJIRA, a package of integrated modules for systematic and interactive analysis of NMR data directed to high-throughput NMR structure studies, J. Biomol. NMR 39 (2007) 31–52.

[21] A. Furukawa, T. Nagata, A. Matsugami, Y. Habu, R. Sugiyama, F. Hayashi, N. Kobayashi, S. Yokoyama, H. Takaku, M. Katahira, Structure, interaction and real-time monitoring of the enzymatic reaction of wild-type APOBEC3G, EMBO J. 28 (2009) 440–451.

[22] T. Nagata, E. Niyada, N. Fujimoto, Y. Nagasaki, K. Noto, Y. Miyanoiri, J. Murata, K. Hiratsuka, M. Katahira, Solution structures of the trihelix DNA-binding domains of the wild-type and a phosphomimetic mutant of Arabidopsis GT-1: mechanism for an increase in DNA-binding affinity through phosphorylation, Proteins 78 (2010) 3033–3047.

[23] D.S. Wishart, B.D. Sykes, The ^{13}C chemical-shift index: a simple method for the identification of protein secondary structure using ^{13}C chemical-shift data, J. Biomol. NMR 4 (1994) 171–180.

[24] C. Zwahlen, P. Legault, S.J.F. Vincent, J. Greenblatt, R. Konrat, L.E. Kay, Methods for measurement of intermolecular NOEs by multinuclear NMR spectroscopy: application to a bacteriophage lambda N-peptide/boxB RNA complex, J. Am. Chem. Soc. 119 (1997) 6711–6721.

[25] E. Katoh, J.M. Louis, T. Yamazaki, A.M. Gronenborn, D.A. Torchia, R. Ishima, A solution NMR study of the binding kinetics and the internal dynamics of an HIV-1 protease–substrate complex, Protein Sci. 12 (2003) 1376–1385.

[26] V. Hornak, A. Okur, R.C. Rizzo, C. Simmerling, HIV-1 protease flaps spontaneously open and reclose in molecular dynamics simulations, Proc. Natl. Acad. Sci. USA 103 (2006) 915–920.

[27] A.L. Perryman, J.H. Lin, J.A. McCammon, Restrained molecular dynamics simulations of HIV-1 protease: the first step in validating a new target for drug design, Biopolymers 82 (2006) 272–284.

[28] A.L. Perryman, Q. Zhang, H.H. Soutter, R. Rosenfeld, D.E. McRee, A.J. Olson, J.E. Elder, C.D. Stout, Fragment-based screen against HIV protease, Chem. Biol. Drug Des. 75 (2010) 257–268.

JOURNAL OF PROTEOMICS 75 (2012) 4863–4873

Available online at www.sciencedirect.com

SciVerse ScienceDirect

www.elsevier.com/locate/jprot

Molecular and enzymatic characterization of XMRV protease by a cell-free proteolytic analysis

Satoko Matsunaga[a], *Tatsuya Sawasaki*[b], *Hirotaka Ode*[c], *Ryo Morishita*[a,d], *Ayako Furukawa*[e], *Ryuta Sakuma*[f], *Wataru Sugiura*[c], *Hironori Sato*[g], *Masato Katahira*[e], *Akifumi Takaori-Kondo*[h], *Naoki Yamamoto*[i], *Akihide Ryo*[a,*]

[a]*Department of Microbiology, Yokohama City University School of Medicine, Yokohama 236-0004, Japan*
[b]*Cell-Free Science and Technology Research Center, Ehime University, Matsuyama 790-8577, Japan*
[c]*Clinical Research Center, National Hospital Organization Nagoya Medical Center, Nagoya 460-0001, Japan*
[d]*CellFree Sciences Co., Ltd., Ehime Univ. Venture Business Laboratory, Matsuyama 790-8577, Japan*
[e]*Institute of Advanced Energy, Kyoto University, Kyoto 611-0011, Japan*
[f]*Department of Molecular Virology, Tokyo Medical and Dental University, Tokyo 113-8510, Japan*
[g]*Pathogen Genomics Center, National Institutes of Infectious Diseases, Tokyo 208-0011, Japan*
[h]*Department of Hematology and Oncology, Graduate School of Medicine, Kyoto University, Kyoto 606-8507, Japan*
[i]*Department of Microbiology, National University of Singapore, Singapore 117597, Singapore*

ARTICLE INFO

Article history:
Received 21 March 2012
Accepted 31 May 2012
Available online 9 June 2012

Keywords:
XMRV
Protease
Cell-free protein synthesis
AlphaSceen

ABSTRACT

Xenotropic murine leukemia virus-related virus (XMRV) is a virus generated under artificial conditions by the recombination of 2 murine leukemia virus (MLV) proviruses, PreXMRV-1 and PreXMRV-2, during the in vivo passage of human prostate cancer cells in athymic nude mice. The molecular etiology of XMRV infection has not been characterized and its implication in human prostate cancer progression remains equivocal. As a step toward resolving this issue we developed an in vitro enzymatic assay system to characterize XMRV protease (PR)-mediated cleavage of host-cell proteins. Enzymatically-active XMRV PR protein was synthesized using a wheat-germ cell-free system. By monitoring cleavage activity of XMRV PR by AlphaScreen and 2-color immunoblot analyses, we revealed that the catalytic activity of XMRV PR is selectively blocked by the HIV PR inhibitor, Amprenavir, and identified several human tumor suppressor proteins, including PTEN and BAX, to be substrates of XMRV PR. This system may provide an attractive means for analyzing the function of retrovirus proteases and provide a technology platform for drug screening.

1. Introduction

Xenotropic murine leukemia virus-related virus (XMRV) was originally isolated from a human prostate cancer (PC) in 2006 [1]. This virus is highly homologous to several endogenous Murine leukemia viruses (MLVs) found in mice [2]. Although previous reports suggested the involvement of XMRV in PC as well as chronic fatigue syndrome (CFS), as an etiological agent, no evidence of this etiological link between XMRV and human disease has been shown to date [3–5].

The nucleotide sequence of XMRV isolated from humans indicates that the virus is nearly identical with the XMRV isolated from the human prostate tumor cell line 22Rv1 [6]. This cell line was generated by serial passage of human prostate tumor tissue in nude mice. Sequence analysis revealed that the genomes of these mouse strains contain two different proviral

* *Corresponding author.* Tel.: +81 45 787 2602; fax: +81 45 787 2851.
E-mail address: aryo@yokohama-cu.ac.jp (A. Ryo).

1874-3919/$ – see front matter
doi:10.1016/j.jprot.2012.05.047

DNAs related to XMRV (Pre-XMRV-1 and 2). It appears that these proviral genomes recombined to produce the XMRV isolated from 22Rv1 cells. It is plausible that the reported association of XMRV with human disease is due to contamination of human samples with virus originating from this recombination event in mice prior to the analysis.

While XMRV arose from an unusual recombination, several lines of study have indicated that XMRV can indeed infect, and proliferate in, several human prostate cancer cell lines including LNCaP and PC3 [7]. It is of significance that dihydrotestosterone (DHT) was shown to stimulate transcription and replication of XMRV through the transactivation of the XMRV-LTR via the hormone response element (HRE) [8]. Mutations in the HRE of XMRV impaired basal transcription and androgen responsiveness, suggesting a relationship between virus productivity and prostatic hypertrophy and neoplasia.

If XMRV is indeed an etiological agent in PCs, detection and elimination of XMRV infection could provide an effective strategy for early diagnosis and treatment of this tumor. To date, however, conflicting epidemiological data has precluded investigations into whether the virus is truly pathogenic or not and, moreover, whether this virus is oncogenic and associated with human PCs.

Retroviral protease (PR) is essential for virus replication and has been the major target for anti-retroviral therapy. Concomitant with particle release, the virally-encoded PR cleaves Gag into its four mature protein domains; MA, CA, NC and p12, in case of XMRV. Gag-Pol is also cleaved by PR, creating the viral enzymes RT, IN and PR itself. The maturation step coupled with PR activation is essential to confer viral infectivity. Therefore, for the effective inhibition of XMRV infection, should this virus be found to be pathogenic, development of anti-retroviral drugs targeting the XMRV protease would seem logical.

Several recent studies have indicated that viral-protease cleavage of host proteins that promotes viral replication and cytopathic effects [9–11]. It remains elusive whether this is the case for XMRV PR. One of the major bottlenecks in PR research has been the difficulty in producing recombinant protein with enzymatic activity in conventional cell-associated protein expression systems (e.g. *E. coli* or insect cell) due to host cell toxicity.

The wheat germ protein production system is a robust in vitro cell-free protein synthesis system comprising a crude wheat germ extract containing ions (buffer) and all the macromolecular components required for protein translation (e.g. ribosomes, tRNAs, aminoacyl-tRNA synthetases, initiation, elongation and termination factors) [12,13]. The extract is further supplemented with amino acids, energy sources such as ATP, energy generating systems and cofactors for efficient and abundant protein production. This system is a powerful tool for the preparation of multiple proteins at one time, and large amounts of specific proteins for both biochemical and biomedical applications. It also enables synthesis of specific proteins that are difficult to express and/or purify in *E. coli* or other cell-based systems. The wheat germ system can produce a wide variety of proteins, including viral proteins, in sufficient amounts for functional assays. Furthermore, this system can yield enzymatically-active proteins in their naturally folded state owing to the constituent eukaryotic translation and folding machinery.

In our current study, we utilized the wheat germ cell-free system to synthesize catalytically active XMRV PR for the identification of potential inhibitors and substrates. By this approach we delineated a molecular link between XMRV PR and human tumor suppressor proteins pointing to a potential role in oncogenesis.

2. Materials and methods

2.1. *Construction of DNA template for transcription and the protein expression*

DNA templates were made using the Gateway and split-primer polymerase chain reaction (PCR) systems [12,14,15]. The tumor suppressor genes were amplified from MGC, a human cDNA resource purchased from Danaform (Tokyo, Japan).

The XMRV protease fragment was amplified by PCR from XMRV VP62 clone [1,16] using the following forward and reverse primers, respectively: (5′-GGGGACAAGTTTGTACAAAAAAGCAGGCTTCATGAAGGACTGCCCAAAGAAGCC-3′) and (5′-GGGGACCACTTTGTACAAGAA AGCTGGGTCTTATAGAGGAACATCTGGCTC-3′). For HIV-1 protease, cDNA fragment was amplified by PCR from HIV-1 NL4-3 clone by using the following forward and reverse primers, respectively: (5′-CCACCCACCACCACCAATGTTTTTTAGGGAAGATC-3′) and (5′-TCCAGCACTAGCTCCAGATTAGCCATCCATTCCTGGC-3′). Subsequently, attB-flanked fragment were amplified by PCR using attB1-S1 primer (5′-GGGGACAAGTTTGTACAAAAAAGCAGGCTTCCACCCACCACCACCAATG-3′) and attB2-T1 primer (5′-GGGGACCACTTTGTACAAGAAAGCTGGGTCTCCAGCACTAGCTCCAGA-3′). The single Capsid (CA) and Nucleocapsid (NC) fragment of XMRV Gag (control substrate), and the 24 tumor suppressor gene fragments (test substrates) were amplified by two-step PCR (without stop codon). The first round of PCR was performed on using 10 nM of S1 (forward) primer (5′- CCACCCACCACCACCAatg(n)19-3′) and T1 (reverse) primer (5′-TCCAGCACTAGCTCCAGA(n)19-3′). The second round of PCR was carried out using the first PCR product as template, with 100nM of attB1-FLAG-S1 (forward) primer (5′-GGGGACAAGTTTGTACAAAAAAGCAGGCTTCATGGACTACAAGGATGACGATGACAAGCTCCACCCACCACCACCAATG-3′) and T1-biotin ligase site (bls)-stop-attB2-anti (reverse) primer (5′-GGGGACCACTTTGTACAAGAAAGCTGGGTTTATTCGTGCCACTCGATCTTCTGGGCCTCGAAGATGTCGTTCAGGCCGCTTCCAGCACTAGCTCCAGA-3′) [17].

The amplified attB-flanked fragments were each inserted into the pDONR221 vector using the Gateway BP Clonase II enzyme mix (Invitrogen, Carlsbad, CA, USA) to give pDONR-XMRV PR vector and pDONR-FLAG-gene-bls vectors, respectively.

pDONR-XMRV PR and pDONR-FLAG-CA/NC-bls vectors were subcloned into pEU-E01-GW [18] to generate the pEU-based-plasmids by LR reaction. BP and LR reactions were performed according to the manufacturer's instructions (Invitrogen). PCR reactions were performed using PrimeStar enzyme according to the manufacturer's instructions (Takara Bio, Otsu, Japan).

For HIV-1 PR substrate, the p2–p7 fragment in HIV-1 Gag precursor was amplified by PCR from HIV-1 NL4-3 clone by using the following forward and reverse primers, respectively: (5′-GAGACTCGAGGCCGAGGCCATGAGCCAGG-3′) and

(5′-GAGCGGTACCTTATTCGTGCCACTCGATCTTCTGGGCCTC-GAAGATGTCGTTCAGGCCATTAGCCTGCCTCTCGGTGCA-3′). The p2–p7-bls fragment was inserted into the pEU-E01-GST-MCS vector (Cellfree Sciences, Yokohama, Japan). The transcription template from pEU vector was amplified using the following forward and reverse primers, respectively: SPu primer (5′-GCGTAGCATTTAGGTGACACT-3′) and AODA2303 (5′-GTCA-GACCCCGTAGAAAAGA-3′). PCR was carried out using the TaKaRa Ex Taq (Takara Bio Inc, Shiga, Japan) according to the manufacturer's instructions.

DNA templates of human genes for transcription were constructed using split-primer PCR in two steps as described previously [18]. For the first step, S1 primers and pDONR221-1st_4080 (5′-ATCTTTTCTACGGGGTCTGA-3′) or AODA2306 (5′- AGCGTCAGACCCCGTAGAAA -3′) were used. For the second step, the primers SPu and pDONR221-2nd_4035 (5′-ACGTTAAGG-GATTTTGGTCA-3′) or AODA2303 were used to generate the final DNA template for transcription.

2.2. *Cell-free protein synthesis*

In vitro transcription and cell-free protein synthesis was performed as described previously [19]. Transcripts were made from each of the DNA templates mentioned above using SP6 RNA polymerase. The synthetic mRNAs were then precipitated with ethanol, collected by centrifugation and washed. Each mRNA (typically 30–35 μg) was added to the translation mixture and the translation reaction was performed in the bilayer mode [20] with slight modifications. The translation mixture that formed the bottom layer consisted of 60 A260 units of wheat germ extract (CellFree Sciences) and 2 μg creatine kinase (Roche Diagnostics K. K., Tokyo, Japan) in 25 μl SUB-AMIX solution (CellFree Sciences). SUB-AMIX contained (final concentrations) 30 mM Hepes/KOH at pH 8.0, 1.2 mM ATP, 0.25 mM GTP, 16 mM creatine phosphate, 4 mM DTT, 0.4 mM spermidine, 0.3 mM each of the 20 amino acids, 2.7 mM magnesium acetate, and 100 mM potassium acetate. SUB-AMIX (125 μl) was placed on the top of the translation mixture, forming the upper layer. After incubation at 16 °C for 16 h, protein synthesis was confirmed by SDS-PAGE. For biotin labeling, 1 μl (50 ng) of crude biotin ligase (BirA) produced by the wheat germ cell-free expression system was added to the bottom layer, and 0.5 μM (final concentration) of D-biotin (Nacalai Tesque, Inc., Kyoto, Japan) was added to both upper and bottom layers, as described previously [21].

2.3. *Detection of cleavage activity of XMRV protease by luminometry*

In vitro cleavage activity assays of XMRV protease were carried out in a total volume of 15 μl consisting of 100 mM Tris–HCl pH 8.0, 0.01% Tween-20, 1 mg/ml BSA, 1 μl crude recombinant protease (~0.75 μM) and 0.5 μl crude recombinant FLAG-biotin-tagged CA/NC (~0.037 μM) at 37 °C for 1 h in a 384-well Optiplate (PerkinElmer, Boston, MA, USA). To assay the effects of HIV protease inhibitors on XMRV protease, after 3 μl recombinant viral protease and HIV protease inhibitor was incubated at 37 °C for 10 min, FLAG-biotin-tagged CA/NC or GST-biotin-tagged p2–p7 was added and the reaction further incubated at 37 °C for 1 h in a 384-well Optiplate. In accordance with the AlphaScreen IgG (Protein A) detection kit (PerkinElmer) instruction manual, 10 μl of detection mixture containing 100 mM Tris–HCl pH 8.0, 0.01% Tween-20, 1 mg/ml BSA, 5 μg/ml Anti-FLAG antibody (Sigma-Aldrich, St. Louis, MO, USA) or Anti-GST antibody (GE Healthcare, Buckinghamshire, UK),, 0.1 μl streptavidin-coated donor beads and 0.1 μl anti-IgG (Protein A) acceptor beads were added to each well followed by incubation at 26 °C for 1 h. Luminescence was analyzed by the AlphaScreen detection program. Each assay was performed in triplicate, and the data represent the means and standard deviations of three independent experiments.

2.4. *Detection of cleavage activity by immunoblotting*

3 μl crude recombinant viral protease (~0.75 μM) and 7 μl crude FLAG-biotin-tagged recombinant proteins were incubated at 37 °C for 2 h. To assay the effect of HIV protease inhibitors, 3 μl crude recombinant XMRV protease and 1 μl of 10 μM HIV protease inhibitor were incubated at 37 °C for 10 min followed by addition of 6 μl crude FLAG-biotin-tagged recombinant proteins, and incubated at 37 °C for 120 min. Proteins were separated by SDS-PAGE and transferred to a PVDF membrane (Millipore Bedford, MA, USA) according to standard procedures. Immunoblot analysis was carried out with anti-FLAG (M2) antibodies (Sigma-Aldrich) or Streptavidin-HRP conjugate (GE Healthcare) according to the procedure described above. For fluorescent imaging, immunoblotted proteins were detected by Alexa592-anti-mouse antibodies (N-cleaved fragments), and Alexa488-streptavidin (C-cleaved fragments). The labeled proteins were visualized using a Typhoon Imager (GE Healthcare).

2.5. *Homology modeling of XMRV PR in complex with APV*

To predict interactions between XMRV PR and APV, we performed homology modeling [22] of the complex structure formed between XMRV PR and APV using the Molecular Operating Environment (MOE) software ver. 2008.10. (Chemical Computing Group, Canada). Firstly, the homologues of XMRV PR were searched for with the MOE-search PDB module from the MOE homology databank. Secondly, to minimize misalignments of the target sequence, multiple alignments were made using sequences of the homologues and those of HIV-1 PR (PDB code: 1HPV) and HTLV PR (PDB code: 3LIN) with the MOE-Align module. The aligned sequences showed that amino acids at the active site of HIV-1, HTLV PRs and those likely to be at the active site of XMRV PR were comparatively conserved, suggesting a structure of HIV-1 PR with APV (PDB code: 1HPV) would be appropriate for a template structure to predict interactions between XMRV PR and APV. Thirdly, homology modeling was performed with MOE-Homology, using the structure of HIV-1 PR in complex with APV (PDB code: 1HPV) as a template structure. During the modeling, the MMFF94x force field and the GB/VI implicit solvent function [23] were applied for energy calculation. In this study, we predicted ten structures of the complex, and selected the structure with the lowest energy as the model for the XMRV PR-APV complex.

3. Results

3.1. Synthesis of an enzymatically active XMRV PR using the wheat germ cell-free system

To synthesize enzymatically-active XMRV PR, we generated a transcription template of this enzyme derived from the XMRV VP62 clone. The template cDNA encodes the open reading frame of XMRV PR flanked by N-terminal 20 amino acid and a C-terminal 20 amino acid regions, as shown in Fig. 1A (PR; 20aa-PR-20aa). This PR differs from the synthesized inactive native PR template by an introduced substitution of the termination codon at the 3′-terminus of the Gag coding sequence for Glu-coding codon (CAG) to avoid translational termination at the end of Gag protein. As a catalytic-incompetent PR, we also designed a PR mutant harboring the catalytic active site substitution D32N (PR_D32N) (Fig. 1A). All 3 cDNA templates were subjected to cell-free transcription-translation. The protein yield of XMRV PR produced by this system was approximately 0.75 μM and the solubility was ~90%, as calculated by semi-quantitative CBB staining following SDS-PAGE (Fig. 1B). By immunoblotting (IB), two specific protein bands appeared at 14 kDa and 17 kDa, corresponding to the expected mobility of the full-length PR and the truncated form of PR by auto-cleavage of the flanking 20 a.a. at both ends (Fig. 1B). The auto-cleavage site of the XMRV PR was also confirmed by amino acid sequencing of the truncated protein band (Fig. 1C).

We next examined the enzymatic activity of the XMRV PR by monitoring its cleavage activity upon a native FLAG-pr55^{Gag} protein substrate. Wheat germ-synthesized XMRV PR was incubated with FLAG-pr55^{Gag} protein followed by immunoblotting analysis. p55^{Gag} was efficiently digested into the expected cleavage products (FLAG-MA-p12 and FLAG-MA) predicted from the known cleavage sites (Fig. 1D).

3.2. Evaluation of protease activity using AlphaScreen

For the quantitative and high-throughput measurement of XMRV PR activity using AlphaScreen technology, we designed a reporter substrate comprising a partial capsid (CA)-nucleo capsid (NC) junction peptide flanked by N-terminal FLAG and C-terminal biotin binding sequence (FLAG-CA/NC-biotin), as described in Materials and methods [14,15]. Fig. 2A shows a schematic representation of our assay system. Briefly, cell-free synthesized active XMRV PR, its D32N mutant or dihydrofolate reductase (DHFR) as a negative control, were incubated with the reporter substrate at 37 °C for 1 h, followed by the addition of AlphaScreen streptavidin donor and protein A acceptor beads as depicted in Fig. 2A. The cleavage of the reporter substrate was measured by level of luminescence (Fig. 2A). Wild-type XMRV PR, but not D32N_PR diminished the Alphascreen luminescent signal indicating proteolytic cleavage of the reporter polypeptide (Fig. 2B). The cleavage activity of PR was normalized relative to the luminescent activity of DHFR (Fig. 2C). Parallel immunoblot analysis with an anti-FLAG antibody demonstrated that the substrate protein was selectively cleaved by PR alone (Fig. 2D).

3.3. Screening of XMRV PR inhibitors by AlphaScreen

We next tested whether our assay system is applicable for drug screening targeting XMVR PR. As an initial approach, we examined the susceptibility of XMRV PR to six HIV-1 PIs: SQV (saquinavir), APV (amprenavir), IDV (indinavir), NFV (nelfinavir), DRV (darunavir) and LPV (lopinavir). Although all HIV-1 PIs tested showed marked inhibitory effects on HIV-1 PR, only two of them, APV and DRV, were found to block the activity of XMRV PR at the 1 μM concentration (Fig. 3A). This was also confirmed by IB of the blockade of cleavage of the reporter polypeptide containing the CA-NC junction (Fig. 3B). We next determined the IC_{50} value by titration of PIs (Fig. 3C). For XMRV PR, the IC_{50} values for APV, DRV, IDV and LPV were 0.2 μM, 1.0 μM, 60 μM and 17 μM, respectively. We next delineate the sensitivity of XMRV PR to APV in comparison with HIV-1 PR. Parallel experiment using recombinant HIV-1 PR and XMRV PR proteins revealed that IC_{50} values for APV was 34.7 nM in HIV PR and 200 nM in XMRV PR, respectively (Fig. 3D). These results indicate that this assay system can provide a tool to screen for selective PR inhibitors.

Retroviruses often exhibit drug resistant properties against anti-retrovirals due to their highly frequent genomic mutation. We next asked whether our assay system is useful for investigating drug-resistant properties of XMRV PR. To predict the sites of interaction between APV and XMRV PR, we modeled the three-dimensional (3D) complex of XMRV PR bound to APV. A recently published report on the crystal structure of XMRV PR shows that XMRV PR has a structural topology similar to that of HIV-1 PR [24]. Thus, we constructed our 3D structural model of the XMRV PR-APV complex by homology modeling, using the X-ray crystal structure of the HIV-1 PR-APV complex as a starting template (Fig. 4A). The constructed model indicates that APV interacts with aspartate Asp32 of the catalytic domain of XMRV PR, and also contacts the residues Val39, Lys61, Tyr90, and Leu92. Moreover, a water molecule would intermediate interactions between APV and Ala57 of the PR. A sequence alignment of PRs between XMRV and HIV-1 shows that the Val39, Ala57, Lys61, Tyr90, and Leu92 in XMRV PR are corresponding to the Val32, Ile50, Ile54, Val82, and Ile84 in HIV-1 PR, respectively (Fig.4B). These residues in HIV-1 PR are reported to be important for interactions between HIV-1 PR and APV and associated with viral resistance against APV [25].

We then created selected site-directed mutants (V39I, K61L, A57V, V39I/A57V, Y90A/L92V) and investigated the catalytic activity and drug-resistant properties of these mutants to APV (Fig. 4C). As shown in Fig. 4C, V39I and A57V substitutions resulted in significantly ($P<0.01$) (Fig. 4C) higher drug resistance as compared with wild-type PR. This effect resulted in the 2.8-fold drug-resistance based on IC_{50} value (Fig.4D). These results indicate that our current assay system can predict drug-susceptibility of mutated proteases and may be useful for drug development targeting XMRV PR.

3.4. Identification of human proteins cleaved by XMRV PR

As it is known that viral proteases can cleave cellular proteins [26–28], we hypothesized that XMRV PR might be capable of digesting human proteins. As a representative demonstration

we selected twenty-four tumor suppressor proteins and synthesized them with N-terminal FLAG and C-terminal biotin tags by wheat cell-free system. These tester proteins were then incubated with XMRV PR followed by 2-color immunoblot analysis (Fig.5B). The result revealed that XMRV PR, but not DHFR as a negative control, can digest 4/24 tumor suppressor proteins examined: BAX, PTEN, DKK3 and ARL11 (Fig. 5C). Cleavage of the tumor suppressor proteins by XMRV PR was clearly inhibited by APV (Fig. 5D). For BAX and PTEN, the cleavage sites by XMRV PR were determined by peptide sequencing of the C-terminal cleavage products (Fig. 5E). The cleavage sites were found to be located in functional domains of both proteins, suggesting that proteolytic digestion by XMRV PR may diminish the native function of these tumor suppressor proteins by proteolytic digestion.

Since XMRV PR and HIV-1 PR have some similarity and can both be inhibited by APV, it is highly possible that XMRV PR can cleave the same substrates as HIV-1 PR. To this end, we tested whether XMRV PR could cleave two reported HIV-1 PR substrates, caspase-8 and NDR2 [28,29]. Interestingly, XMRV PR was found to digest caspase-8 although the cleavage site was distinct from that of HIV-1 PR. In contrast, XMRV PR was not able digest NDR2. Conversely, HIV-1 PR did not cleave Bax whereas XMRV PR can cleave it. Furthermore, both proteases could not cleave p53. These results indicate that there is certain substrate specificity of retroviral proteases toward host proteins (Fig. 6).

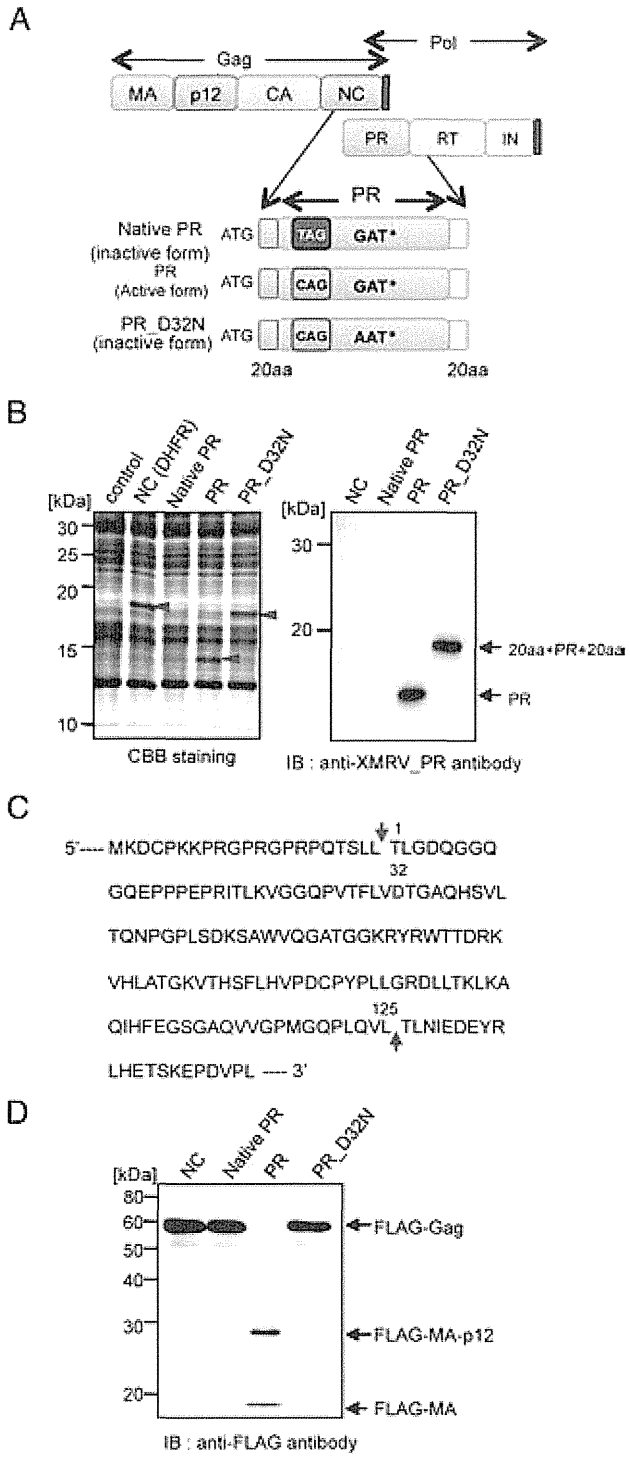

Fig. 1 – Synthesis of enzymatically active XMRV protease (PR) by wheat cell-free protein production system. A. Construction of expression vector of XMRV PR for wheat cell-free synthesis. TAG (stop) codon between Gag and PR was substituted for CAG (Q) codon. Non-active form of PR was generated by the substitution of AAT (N) for catalytic center GAT (D). B. XMRV PRs (DHFR as a negative control) were separated by SDS-PAGE followed by CBB-stained (left panel) and immunoblotting using anti-XMRV PR antibody (right). The arrows depict protein products. C. Amino acid sequence of XMRV PR. The arrows indicate self-cleavage site in XMRV PR. D. Cleavage of XMRV Gag by XMRV PR produced by wheat cell-free system. XMRV PR was incubated with cell-free synthesized FLAG-tagged XMRV Gag (arrow), and the cleaved Gag was detected by immunoblot analysis with anti-FLAG antibody.

4. Discussion

In the current study, we developed a cell free protease assay with XMRV PR which can evaluate the cleavage activity via AlphaScreen or immunoblot analysis. We demonstrate the advantage of utilizing wheat cell-free system that was able to systematically produce catalytically active viral protease with a large amount for biochemical assays. Furthermore, our in vitro enzymatic assay revealed that APV is a potent inhibitor of XMRV PR. We have also delineated the physical interaction between APV and XMRV PR and identified the amino acid residues involved in the binding. Finally, we demonstrated the substrate specificity for XMRV PR as compared with HIV-1 PR. These results might reveal that our current assay system is a powerful tool to characterize viral proteases and to screen their specific inhibitors.

XMRV is a virus that was generated as the result of a unique recombination event between two endogenous MLV-like viruses in a nude mouse carrying the CWR22 prostate cancer xenograft [6]. Although XMRV is an unusual virus, XMRV has been associated with prostate cancer [2]. In fact, the human cell line 22Rv1, which was established from a human prostate tumor (CWR22), produces infectious XMRV particles [30]. While the absence of XMRV in non-prostatic tumors

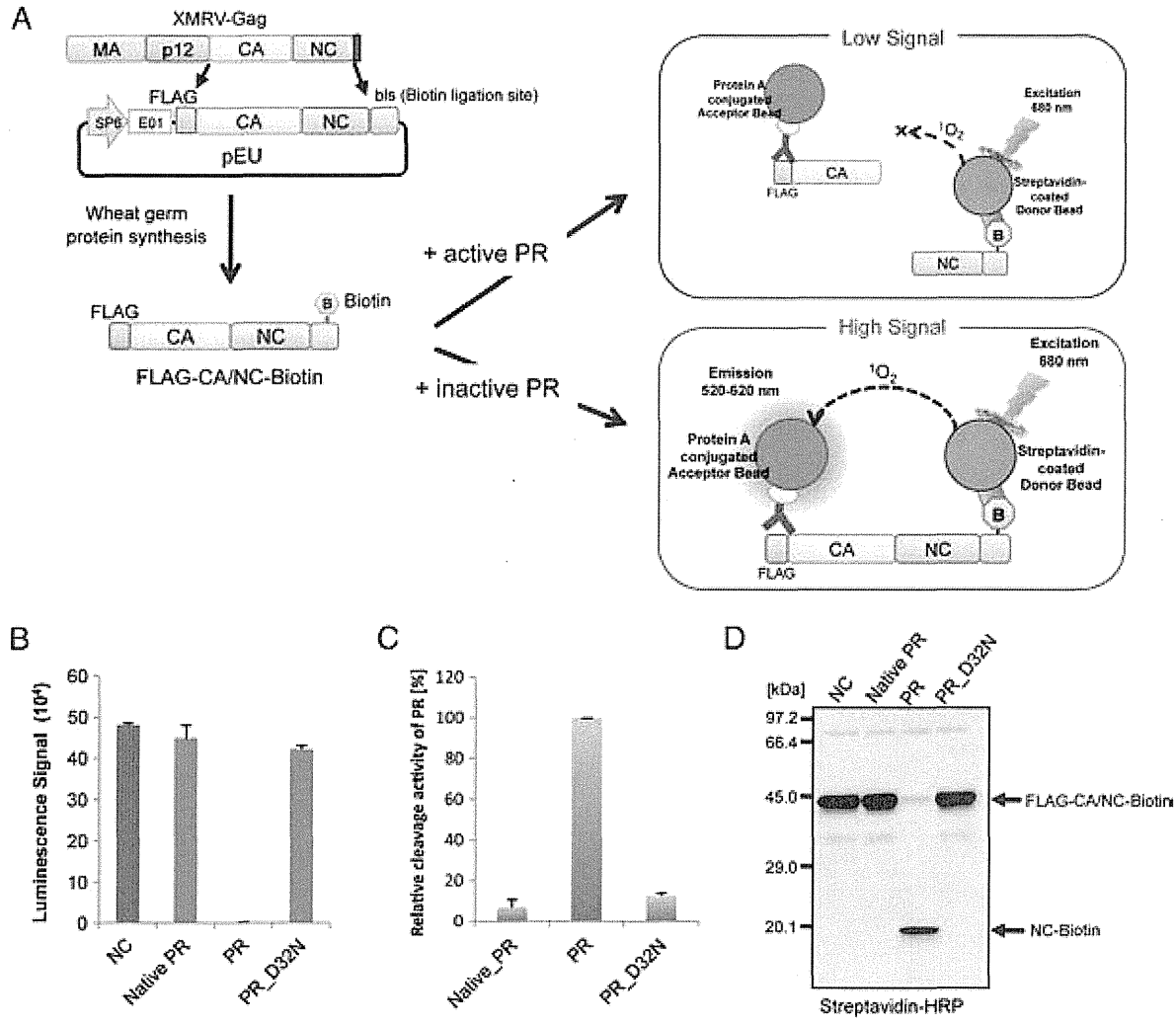

Fig. 2 – Development of a cleavage activity assay for XMRV PR using the luminescent assay AlphaScreen. A. Schematic diagram of the substrate construction of XMRV PR and detection system for the cleavage activity of XMRV PR by luminescent analysis. Substrate was designed as XMRV Gag capside (CA) and nucleocapsid (NC) flanked by N-terminal FLAG and C-terminal biotin (FLAG_CA-NC_biotin). PR was incubated with the substrate, for 1 h at 37 °C. Subsequently, protein A-conjugated acceptor beads with anti-FLAG antibody and streptavidin coated donor beads were added and bound to the tagged substrate. Upon laser excitation, Donor beads convert ambient oxygen to a singlet oxygen. In the case of non-activity PR, singlet oxygen transfers across to activate Acceptor beads and subsequently emit light at 520–620 nm. In the case of active PR, no light is produced because the singlet oxygen can not transfer from Donor beads to Acceptor beads due to the distance (>200 nm). B,C,D. Cleavage activity of XMRV PR was quantitated by the luminescent assay (Fig.2B). Actual cleavage of XMRV Gag substrate was also confirmed by immunoblotting with streptavidin-HRP (Fig.2D). The arrow indicates the band for the non-cleaved substrates (FLAG_CA/NC_biotin).

remains controversial [31], XMRV can however proliferate in other human prostate cancer cells such as LNCaP or PC3 without severe cytopathic effects [32]. Such conditions of persistent infection without cell death could conceivably lead to prolonged exposure of host cell proteins to XMRV PR, increasing their susceptibility to cleavage with oncogenic consequences. The important question remains, however, as to whether this virus has indeed tumorigenic capability. Previous reports have indicated that XMRV integration is characterized by a strong preference for transcriptional start sites, CpG islands, and DNase-hypersensitive regions, all features that are frequently associated with structurally-open transcription regulatory regions of the chromosome in prostate cancer cells [33]. Integration of XMRV occurs preferentially in actively-transcribed genes and gene-dense regions within the chromosome [33]. Oncogenic properties of XMRV have been investigated in cell culture models. Although XMRV has been reported to lack direct transforming activity, the virus is able to induce low rates of transformation in cultured fibroblast cells [34]. Therefore, the molecular link between XMRV infection and cell transformation merits further investigation.

Our current data demonstrates that APV is a potent antagonist of XMRV PR. During the preparation of this manuscript, Li et al. reported the crystal structure of complexes

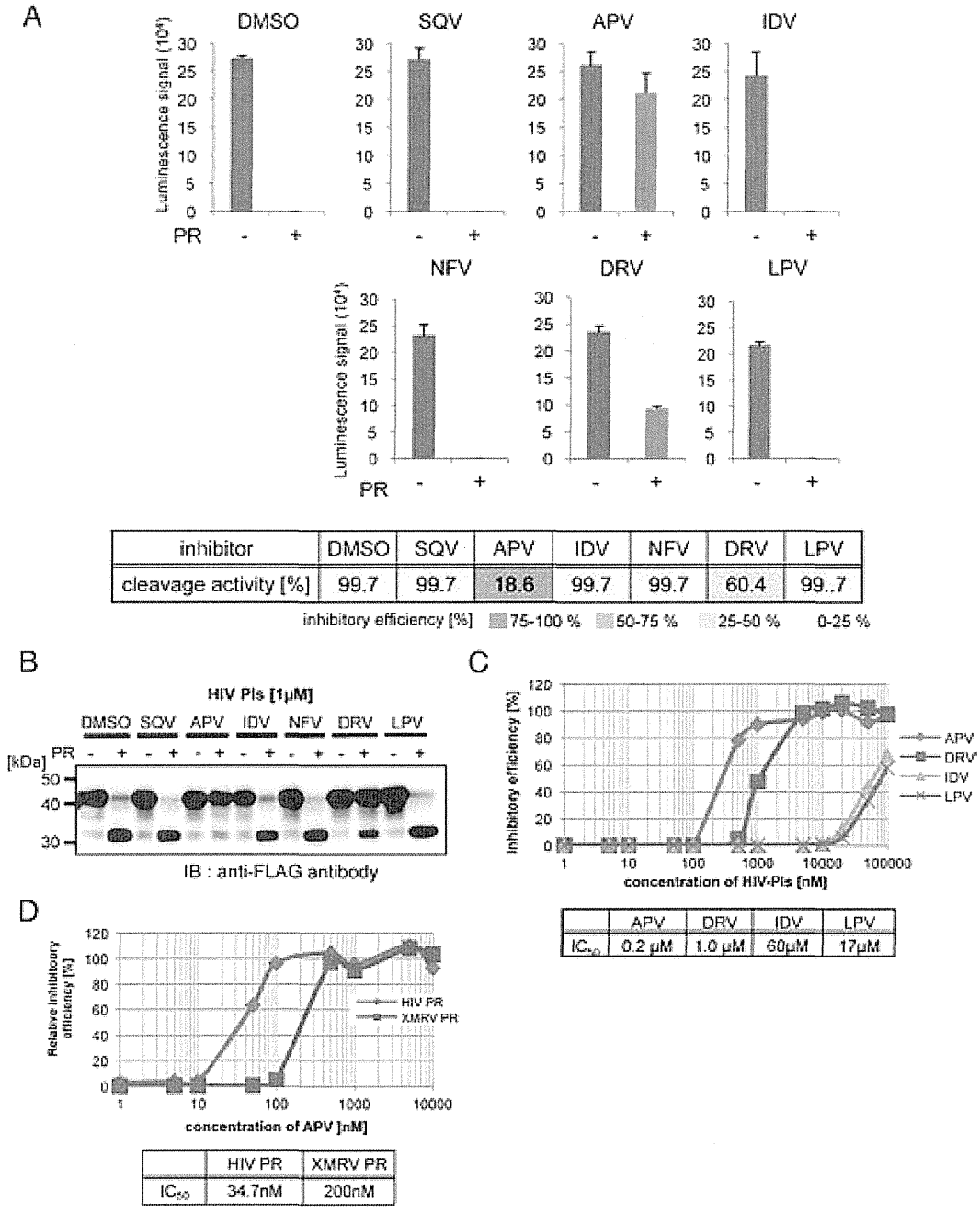

Fig. 3 – Drug screening for XMRV PR based on the cleavage activity. A,B. XMRV protease (+) or DHFR (–) was pre-incubated with indicated HIV PIs (SQV, saquinavir; APV, amprenavir; IDV, indinavir; NFV, nelfinavir ; DRV, darunavir; LPV, lopinavir; 1 μM each) and then subjected to AlphaScreen. Luminiscent AlphaScreen signal (upper panel) and relative enzymatic activity (lower panel) were listed. C. Conformation of the cleavage of the tester polypeptide by immunoblot analysis with anti-FLAG antibody. D. Dose–response curve of XMRV PR with HIV PIs using AlphaScreen (upper panel). IC_{50} values were calculated for each inhibitor (lower panel). E. Dose–response curve of XMRV PR and HIV-1 PR with APV using AlphaScreen (upper panel). IC_{50} values were calculated for each protease (lower panel).

formed between XRMV PR and several protease inhibitors, including APV [24,35]. In the current study we moved a step closer to clarifying the molecular interactions between XMRV PR and APV during drug-resistance, by developing an effective cell-free in vitro protease assay for XMRV PR. This assay revealed that an Ala57Val substitution induced significant drug-resistance to APV regardless of the integrity of the protease activity. The data indicates that this cell-free assay is useful for analyzing the drug-resistance properties of retroviral proteases.

Proteases often modify the activities of their target substrates [36]. Identification of the specific substrates cleaved by viral PR is of great significance for understanding the molecular etiology of virus infection. Proteomic studies with mass spectrometry could, theoretically, exhaustively identify the cellular proteins cleaved

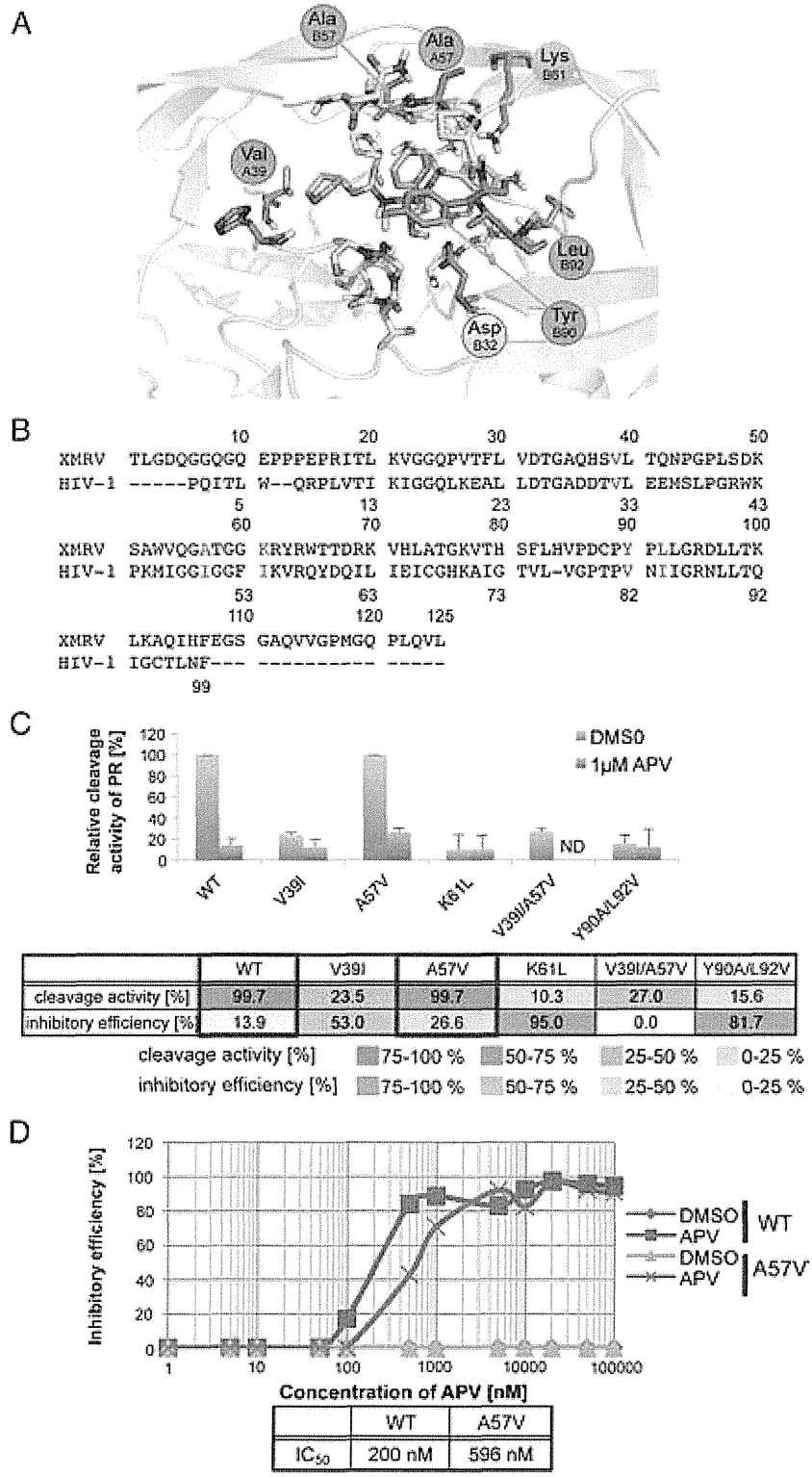

	WT	V39I	A57V	K61L	V39I/A57V	Y90A/L92V
cleavage activity [%]	99.7	23.5	99.7	10.3	27.0	15.6
inhibitory efficiency [%]	13.9	53.0	26.6	95.0	0.0	81.7

	WT	A57V
IC_{50}	200 nM	596 nM

Fig. 4 – Prediction of the amino acid residues of XMRV PR interacting with APV. A. The predicted 3D-structure for the interaction between XMRV PR and APV. This homology modeling was based on the HIV-1 PR and APV complex as a template. B. Sequence alignment of XMRV PR and HIV-1 PR. The amino acids related to interaction of APV with HIV-1 PR and the corresponding amino acids in XMRV PR are highlighted with red letters. C. Cleavage activity of XMRV PR-WT and its mutants in the presence of 1 μM APV or equivalent amount of DMSO (control). Lower panel is cleavage activity and inhibitory efficiency (APV value/DMSO value) for each XMRV PR. D. Dose–response curve of the inhibitory rate of PR-WT or PR-A57V by APV.

A

No.	Symbol	Gene bank accession No.	aa	Da	Cleavage by XMRV PR
1	ANXA1	BC001275	346	38714	No
2	GJB2	BC017048	226	26215	No
3	ARL11	BC013150	196	21391	Yes
4	RND3	BC012513	244	27368	No
5	FHIT	BC032336	147	16858	No
6	KCNRG	BC032343	272	31048	No
7	SFRP1	BC036503	314	35386	No
8	WNT5A	BC064694	380	42339	No
9	SMAD3	BC050743	425	48081	No
10	p21	BC000312	164	18119	No
11	NME1	BC000293	152	17149	No
12	MAL	BC000458	153	16714	No
13	SPINT2	BC001668	252	28228	No
14	SLC39A1	BC003152	324	34250	No
15	CHEK2	BC004207	543	60916	No
16	DKK3	BC007660	350	38291	Yes
17	TIMP3	BC014277	211	24145	No
18	BAX	BC014175	192	21184	Yes
19	ALPL	BC021289	524	57305	No
20	CST6	BC031334	149	16510	No
21	KLF5	BC042131	457	50792	No
22	CAV1	BC082246	178	20472	No
23	PTEN	BC005821	403	47166	Yes
24	TP53	BC003596	393	43653	No

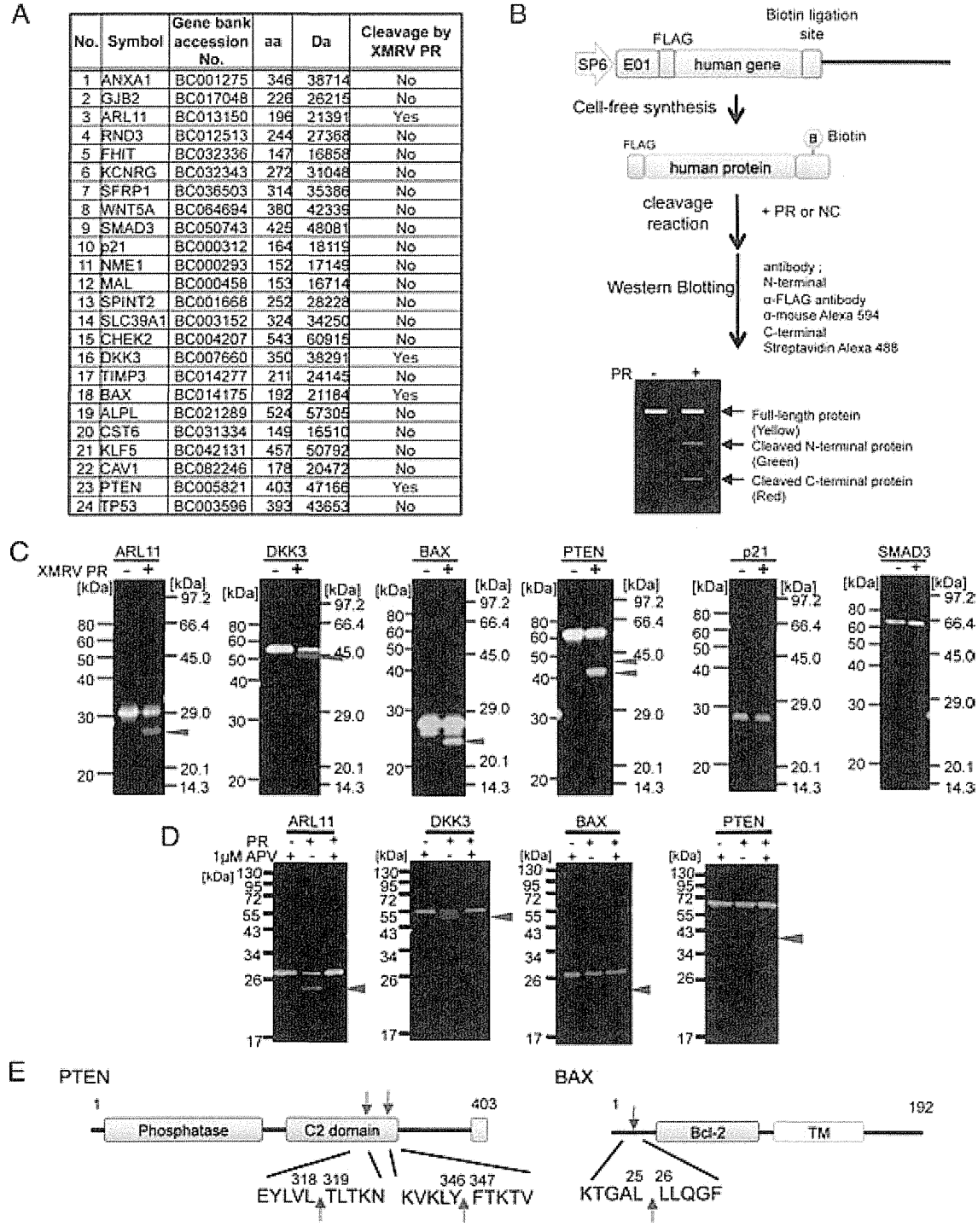

Fig. 5 – Screening of host proteins cleaved by XMRV PR in vitro. A. The list of human tumor suppressor proteins tested in this study. B. Scheme of the tester proteins construction and the cleavage assay system by immunoblotting. The genes were amplified by PCR with primer sets containing either FLAG or biotin ligation site (bls) in the flanking sequence, respectively. The recombinant host proteins flanking FLAG and biotin (FLAG-X-biotin) were incubated with XRMV PR at 37 °C for 2 h followed by SDS-PAGE. The proteins were detected using anti-FLAG-Alexa592 antibody (green) and Alexa488-conjugated streptavidin (red). Full-length protein is seen as a yellow band. C. Tester proteins were treated with XMRV PR or carrier. 2-color immunoblot analysis was performed as in Materials and methods. D. Tester proteins were treated with XMRV PR in the absence or presence of amprenavir. Immunoblot analysis was performed as in C. E. Identification of the cleavage site in the XMRV PR amino acid sequence.

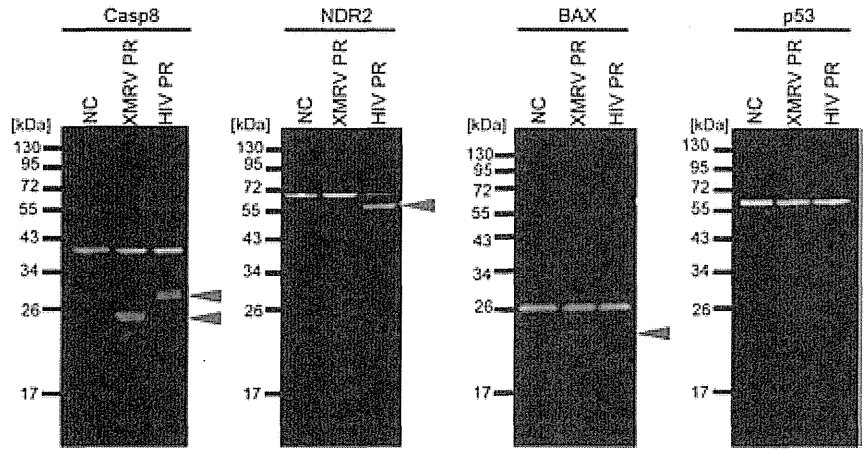

Fig. 6 – Comparative analysis of host proteins cleaved by XMRV PR and HIV-1 PR. The recombinant host proteins flanking FLAG and biotin (FLAG-X-biotin) were incubated with either XRMV PR or HIV-1 PR at 37 °C for 2 h followed by SDS-PAGE. The proteins were detected using anti-FLAG-Alexa592 antibody (green) and Alexa488-conjugated streptavidin (red). Full-length protein is seen as a yellow band. Arrows depict the cleavage products.

by retroviral proteases in infected cells. However, this cell-based will run into difficulty identifying individual substrates if several host proteases act simultaneously on the substrate. To circumvent this potential problem we developed the cell-free in vitro method for the identification of substrates cleavable by XMRV PR. Wheat extracts purified rarely include endogenous proteases that can interfere with the proteolytic reaction, making them suitable for the cell-free protease assay.

Tumor suppressor proteins play a major role in preventing tumor initiation. Our current results demonstrate that XMRV PR can cleave PTEN and BAX tumor suppressors as well as the intrinsic substrate XMRV Gag. It has been reported that the C-terminal region of PTEN is important for the protein's stability, and the C-terminal deletion mutant is degraded rapidly in cells [37]. Since XMRV cleaves within the C-terminal region, the native function and stability of PTEN might be abrogated by XMRV infection. The N-terminal region of BAX has been demonstrated to mediate its activity in apoptosis [38]. We demonstrated in the present study that XMRV PR can cleave the N-terminal region of BAX, suggesting that XMRV infection might affect the activity of BAX protein.

A biochemical approach to the evaluation of PR-inhibitor susceptibility has been attempted previously using several related methods [39,40]. The essence of each of these procedures is the synthesis of catalytically-active PR and substrate peptide and inhibitor in vitro, and measurement of the amount of substrate cleavage. The advantage of this approach is that it can directly detect the catalytic activity of PR. However, it is often difficult to produce sufficient quantities of enzymatically active viral PR in conventional cell-based protein expression systems such as *E. coli* or insect cells. In our current study, we successfully created catalytically-active XMRV PR in a cell-free system that, when mixed with a reporter substrate flanked with N- and C-terminal fluorophores, substrate cleavage could be assayed by AlphaScreen or 2-color IB. This approach directly evaluates the cleavage activity of the PR and, in addition, cleavage sites can be estimated by the size of cleavage products. The current availability of full-length cDNA libraries, derived from higher eukaryotes, will facilitate the in vitro synthesis of full-length proteins, making this cell-free system approach could further be applicable to the assay of a broad range of, not only viral, but also host proteases.

5. Conclusion

We have delineated the molecular and enzymatic characteristics of XMRV PR by utilizing wheat-germ cell-free protein synthesis and AlphaScreen. Furthermore, we have developed an in vitro cleavage assay for drug screening based on the enzymatic activity. Our results suggest that XMRV-protease cleavage of certain host proteins and inhibited by APV. Further in vivo studies with XMRV-infected cells will be necessary to confirm a molecular link between XMRV and human diseases.

Acknowledgments

We thank Drs. G. Quinn, Y. Kojima and A. Kudo for the discussion and comments. This work was supported in part by grants from the Ministry of Education, Culture, Sports, Science and Technology of Japan and Research Grants on HIV/AIDS Health Labour Sciences Research Grant from The Ministry of Health Labour and Welfare of Japan to A.R. MK was supported by grants from MEXT, JST, Sumitomo-Denko and Iwatani.

REFERENCES

[1] Urisman A, Molinaro RJ, Fischer N, Plummer SJ, Casey G, Klein EA, et al. Identification of a novel Gammaretrovirus in prostate tumors of patients homozygous for R462Q RNASEL variant. PLoS Pathog 2006;2:e25.

[2] Schlaberg R, Choe DJ, Brown KR, Thaker HM, Singh IR. XMRV is present in malignant prostatic epithelium and is

associated with prostate cancer, especially high-grade tumors. Proc Natl Acad Sci U S A 2009;106:16351–6.
[3] Knox K, Carrigan D, Simmons G, Teque F, Zhou Y, Hackett Jr J, et al. No evidence of murine-like gammaretroviruses in CFS patients previously identified as XMRV-infected. Science 2011;333:94–7.
[4] van Kuppeveld FJ, van der Meer JW. XMRV and CFS–the sad end of a story. Lancet 2012;379:e27–8.
[5] Simmons G, Glynn SA, Komaroff AL, Mikovits JA, Tobler LH, Hackett Jr J, et al. Failure to confirm XMRV/MLVs in the blood of patients with chronic fatigue syndrome: a multi-laboratory study. Science 2011;334:814–7.
[6] Paprotka T, Delviks-Frankenberry KA, Cingoz O, Martinez A, Kung HJ, Tepper CG, et al. Recombinant origin of the retrovirus XMRV. Science 2011;333:97–101.
[7] Groom HC, Yap MW, Galao RP, Neil SJ, Bishop KN. Susceptibility of xenotropic murine leukemia virus-related virus (XMRV) to retroviral restriction factors. Proc Natl Acad Sci U S A 2010;107:5166–71.
[8] Dong B, Silverman RH. Androgen stimulates transcription and replication of xenotropic murine leukemia virus-related virus. J Virol 2010;84:1648–51.
[9] Abudu A, Takaori-Kondo A, Izumi T, Shirakawa K, Kobayashi M, Sasada A, et al. Murine retrovirus escapes from murine APOBEC3 via two distinct novel mechanisms. Curr Biol 2006;16:1565–70.
[10] Ventoso I, Blanco R, Perales C, Carrasco L. HIV-1 protease cleaves eukaryotic initiation factor 4G and inhibits cap-dependent translation. Proc Natl Acad Sci U S A 2001;98:12966–71.
[11] Zaragoza C, Saura M, Padalko EY, Lopez-Rivera E, Lizarbe TR, Lamas S, et al. Viral protease cleavage of inhibitor of kappaBalpha triggers host cell apoptosis. Proc Natl Acad Sci U S A 2006;103:19051–6.
[12] Takai K, Sawasaki T, Endo Y. Practical cell-free protein synthesis system using purified wheat embryos. Nat Protoc 2010;5:227–38.
[13] Kamura N, Sawasaki T, Kasahara Y, Takai K, Endo Y. Selection of 5′-untranslated sequences that enhance initiation of translation in a cell-free protein synthesis system from wheat embryos. Bioorg Med Chem Lett 2005;15:5402–6.
[14] Tadokoro D, Takahama S, Shimizu K, Hayashi S, Endo Y, Sawasaki T. Characterization of a caspase-3-substrate kinome using an N- and C-terminally tagged protein kinase library produced by a cell-free system. Cell Death Dis 2010;1:e89.
[15] Akagi T, Shimizu K, Takahama S, Iwasaki T, Sakamaki K, Endo Y, et al. Caspase-8 cleavage of the interleukin-21 (IL-21) receptor is a negative feedback regulator of IL-21 signaling. FEBS Lett 2011;585:1835–40.
[16] Sakuma R, Sakuma T, Ohmine S, Silverman RH, Ikeda Y. Xenotropic murine leukemia virus-related virus is susceptible to AZT. Virology 2010;397:1–6.
[17] Sawasaki T, Kamura N, Matsunaga S, Saeki M, Tsuchimochi M, Morishita R, et al. Arabidopsis HY5 protein functions as a DNA-binding tag for purification and functional immobilization of proteins on agarose/DNA microplate. FEBS Lett 2008;582:221–8.
[18] Takahashi H, Nozawa A, Seki M, Shinozaki K, Endo Y, Sawasaki T. A simple and high-sensitivity method for analysis of ubiquitination and polyubiquitination based on wheat cell-free protein synthesis. BMC Plant Biol 2009;9:39.
[19] Sawasaki T, Gouda MD, Kawasaki T, Tsuboi T, Tozawa Y, Takai K, et al. The wheat germ cell-free expression system: methods for high-throughput materialization of genetic information. Methods Mol Biol 2005;310:131–44.
[20] Sawasaki T, Hasegawa Y, Tsuchimochi M, Kamura N, Ogasawara T, Kuroita T, et al. A bilayer cell-free protein synthesis system for high-throughput screening of gene products. FEBS Lett 2002;514:102–5.
[21] Matsuoka K, Komori H, Nose M, Endo Y, Sawasaki T. Simple screening method for autoantigen proteins using the N-terminal biotinylated protein library produced by wheat cell-free synthesis. J Proteome Res 2010;9:4264–73.
[22] Baker D, Sali A. Protein structure prediction and structural genomics. Science 2001;294:93–6.
[23] Labute P. The generalized Born/volume integral implicit solvent model: estimation of the free energy of hydration using London dispersion instead of atomic surface area. J Comput Chem 2008;29:1693–8.
[24] Li M, Dimaio F, Zhou D, Gustchina A, Lubkowski J, Dauter Z, et al. Crystal structure of XMRV protease differs from the structures of other retropepsins. Nat Struct Mol Biol 2011;18:227–9.
[25] Johnson VA, Brun-Vezinet F, Clotet B, Gunthard HF, Kuritzkes DR, Pillay D, et al. Update of the drug resistance mutations in HIV-1. Top HIV Med 2008;16:138–45.
[26] Alvarez E, Castello A, Menendez-Arias L, Carrasco L. HIV protease cleaves poly(A)-binding protein. Biochem J 2006;396:219–26.
[27] Bellecave P, Sarasin-Filipowicz M, Donze O, Kennel A, Gouttenoire J, Meylan E, et al. Cleavage of mitochondrial antiviral signaling protein in the liver of patients with chronic hepatitis C correlates with a reduced activation of the endogenous interferon system. Hepatology 2010;51:1127–36.
[28] Nie Z, Phenix BN, Lum JJ, Alam A, Lynch DH, Beckett B, et al. HIV-1 protease processes procaspase 8 to cause mitochondrial release of cytochrome c, caspase cleavage and nuclear fragmentation. Cell Death Differ 2002;9:1172–84.
[29] Devroe E, Silver PA, Engelman A. HIV-1 incorporates and proteolytically processes human NDR1 and NDR2 serine-threonine kinases. Virology 2005;331:181–9.
[30] Knouf EC, Metzger MJ, Mitchell PS, Arroyo JD, Chevillet JR, Tewari M, et al. Multiple integrated copies and high-level production of the human retrovirus XMRV (xenotropic murine leukemia virus-related virus) from 22Rv1 prostate carcinoma cells. J Virol 2009;83:7353–6.
[31] Stieler K, Schindler S, Schlomm T, Hohn O, Bannert N, Simon R, et al. No detection of XMRV in blood samples and tissue sections from prostate cancer patients in Northern Europe. PLoS One 2011;6:e25592.
[32] Rodriguez JJ, Goff SP. Xenotropic murine leukemia virus-related virus establishes an efficient spreading infection and exhibits enhanced transcriptional activity in prostate carcinoma cells. J Virol 2010;84:2556–62.
[33] Kim S, Kim N, Dong B, Boren D, Lee SA. Das Gupta J, et al. Integration site preference of xenotropic murine leukemia virus-related virus, a new human retrovirus associated with prostate cancer. J Virol 2008;82:9964–77.
[34] Metzger MJ, Holguin CJ, Mendoza R, Miller AD. The prostate cancer-associated human retrovirus XMRV lacks direct transforming activity but can induce low rates of transformation in cultured cells. J Virol 2010;84:1874–80.
[35] Li M, Gustchina A, Matuz K, Tozser J, Namwong S, Goldfarb NE, et al. Structural and biochemical characterization of the inhibitor complexes of xenotropic murine leukemia virus-related virus protease. FEBS J 2011;278:4413–24.
[36] Etlinger JD, Gu M, Li X, Weitman D, Rieder RF. Protease/inhibitor mechanisms involved in ATP-dependent proteolysis. Rev Biol Cell 1989;20:197–216.
[37] Georgescu MM, Kirsch KH, Akagi T, Shishido T, Hanafusa H. The tumor-suppressor activity of PTEN is regulated by its carboxyl-terminal region. Proc Natl Acad Sci U S A 1999;96:10182–7.
[38] Toyota H, Yanase N, Yoshimoto T, Moriyama M, Sudo T, Mizuguchi J. Calpain-induced Bax-cleavage product is a more potent inducer of apoptotic cell death than wild-type Bax. Cancer Lett 2003;189:221–30.
[39] Dreyer GB, Metcalf BW, Tomaszek Jr TA, Carr TJ, Chandler 3rd AC, Hyland L, et al. Inhibition of human immunodeficiency virus 1 protease in vitro: rational design of substrate analogue inhibitors. Proc Natl Acad Sci U S A 1989;86:9752–6.
[40] Hoffmann D, Buchberger B, Nemetz C. In vitro synthesis of enzymatically active HIV-1 protease for rapid phenotypic resistance profiling. J Clin Virol 2005;32:294–9.